Iron affects Ire1 clustering propensity and the amplitude of endoplasmic reticulum stress signaling.

Nir Cohen[1]*, Michal Breker[1,2]*, Anush Bakunts[3], Kristina Pesek[4], Ainara Chas[5], Josepmaria Argemí[5], Andrea Orsi[3], Lihi Gal[1], Silvia Chuartzman[1], Yoav Wigelman[1], Felix Jonas[1], Peter Walter[6], Robert Ernst[7], Tomás Aragón[5], Eelco van Anken[3] & Maya Schuldiner[1]

* These authors contributed equally to this work.

Correspondence should be addressed to: vananken.eelco@hsr.it; maya.schuldiner@weizmann.ac.il

1. Department of Molecular Genetics, Weizmann Institute of Science, Rehovot 7610001, Israel
2. The Rockefeller University, New York, NY
3. San Raffaele Scientific Institute, Ospedale San Raffaele, Via Olgettina 58, 20132, Milan, Italy
4. Institute of Biochemistry and Buchmann Institute for Molecular Life Sciences, Goethe University Frankfurt, Max-von-Laue Str. 15, 60438 Frankfurt, Germany
5. Department of Gene Therapy and Regulation, Center for Applied Medical Research, University of Navarra. 55 Pio XII St. 31008 Pamplona, Spain.
6. Department of Biochemistry & Biophysics, University of California San Francisco and Howard Hughes Medical Institute, San Francisco, CA 94143, USA
7. Institute of Medical Biochemistry and Molecular Biology, Saarland University, 66421 Homburg, Germany.

Running Title: Iron affects Ire1 clustering

Keywords: Ire1, Iron, Heme, Sterol, *Saccharomyces cerevisiae*, UPR

Summary statement: To respond to folding stress in the endoplasmic reticulum cells activate the conserved sensor Ire1. We show that iron is required for optimal Ire1 activation and suggest ergosterol biosynthesis as the reason.

Abstract:

The unfolded protein response (UPR) allows cells to adjust secretory pathway capacity according to need. Ire1, the endoplasmic reticulum (ER) stress sensor and central activator of the UPR is conserved from the budding yeast *Saccharomyces cerevisiae* to humans. Under ER stress conditions, Ire1 clusters into foci that enable optimal UPR activation. To discover factors that affect Ire1 clustering, we performed a high-content screen using a whole-genome yeast mutant library expressing Ire1-mCherry. We imaged the strains following UPR induction and found 154 strains that displayed alterations in Ire1 clustering. The hits were enriched for iron and heme effectors and binding proteins. By pharmacological depletion and repletion, we confirmed that iron affects UPR activation in both yeast and human cells. We suggest that Ire1 clustering propensity depends on membrane composition, which is governed by heme-dependent biosynthesis of sterols. Our findings highlight the diverse cellular functions that feed into the UPR and emphasize the cross-talk between organelles required to concertedly maintain homeostasis.

Introduction

The unfolded protein response (UPR) is a homeostatic response pathway that adjusts the endoplasmic reticulum (ER) protein folding capacity according to need. The UPR is common to all eukaryotes despite variance in sensing machineries and regulation (Walter and Ron, 2011). The UPR signaling mechanism that is initiated by Ire1 is present from *Saccharomyces cerevisiae* (from here on referred to simply as "yeast") to humans (Cox et al., 1993; Mori et al., 1993; Tirasophon et al., 1998; Walter and Ron, 2011). Ire1 is a single pass ER membrane protein that senses stress such as the accumulation of misfolded proteins (Cox et al., 1997) or alterations in membrane composition (Halbleib et al., 2017; Pineau et al., 2009; Promlek et al., 2011; Surma et al., 2013). Upon activation, Ire1 dimerizes to activate its kinase domain in the cytosol and trans autophosphorylates (Shamu and Walter, 1996; Tirasophon et al., 1998). Phosphorylation activates Ire1's endonuclease domain driving a non-conventional splicing reaction, which removes a single intron from *HAC1* mRNA in yeast (Cox and Walter, 1996; Yoshida et al., 1998) and its orthologous *XBP1* mRNA in mammals (Yoshida et al., 2001). The splicing reaction enables the creation of the mature proteins, which act as transcription factors for genes promoters encode a UPR element (UPRE) in yeast (Cox and Walter, 1996) or an ER stress element (ERSE) in mammals (Yoshida et al., 1998).

Over the last years it has become evident that both Ire1 and Hac1/Xbp1 are regulated on multiple levels (Gardner et al., 2013; Pineau et al., 2009). One regulatory aspect of Ire1 function is its propensity to cluster into foci upon ER stress in both yeast (Aragón et al., 2009; Kimata et al., 2007; van Anken et al., 2014) and mammals (Li et al., 2010). While this clustering is not essential for UPR initiation is has a role in enabling optimal activation (Li et al., 2010) by providing a platform to which the *HAC1* mRNA can be targeted (Aragón et al., 2009) and docked (van Anken et al., 2014), ensuring efficiency and specificity of the splicing reaction (van Anken et al., 2014).

We decided to exploit formation of Ire1 clusters as a striking visual output for the extent of UPR activation and set out to perform a high content screen using a library of yeast strains in which single genes were ablated or had reduced function. We found that the loss of many genes affected the dynamics of Ire1 clustering. Surprisingly, the hits were highly enriched in genes associated with iron and heme metabolism. In line with the genetic evidence, we showed that iron availability strongly influenced whether a productive UPR could be mounted in both yeast and human cells. We continued to show that heme and ergosterol biosynthesis enzymes are required for optimal clustering. We thus raise the hypothesis that iron levels affect heme biosynthesis that, in turn, determines membrane composition (since heme is a co-factor of enzymes in sterol biosynthesis as well as enzymes that affect lipid saturation), and that membrane composition affects Ire1 clustering. Our findings support previous observations on the role of membrane composition in UPR activation (Volmer and Ron, 2015) as well as our recent observations on how Ire1 senses bilayer stress (Halbleib et al., 2017). Thus, iron and heme levels, next to ATP levels (McClellan et al., 1998; Todd-Corlett et al., 2007), the level of unfolded proteins in the ER lumen (Gardner and Walter, 2011; McClellan et al., 1998; Todd-Corlett et al., 2007) and the extent of BiP (Kar2 in yeast) binding to Ire1 (Okamura et al., 2000; Todd-Corlett et al., 2007) are all determinants of Ire1 activation and thereby can play a role in the fine-tuning of the UPR.

Results

A high content screen uncovers multiple effectors of Ire1 clustering

To monitor the dynamics of UPR activation through visualization of Ire1 clustering we created a yeast strain expressing Ire1 that is tagged with mCherry in the cytosolic linker that tethers Ire1's

kinase domain to the transmembrane region. This unique tag localization preserves all Ire1 functions (Aragón et al., 2009). We confirmed that Ire1-mCherry, when exposed to the reducing agent dithiothreitol (DTT) that induces ER stress, redistributed from its diffuse localization throughout the ER membrane into small discrete punctate structures that were easy to visualize after 2 hours. The Ire1-mCherry foci then grew in size and Ire1-mCherry remained clustered for the entire duration of the experiment, spanning over more than 10 hours (Figure 1A).
To measure how such localization dynamics relate to downstream UPR activation, we also employed a strain that harbors the UPRE-GFP reporter cassette (Cox and Walter, 1996). In this strain, GFP fluorescence can be used as a proxy for the extent of UPR activation. Indeed, by 2 hours post DTT addition we could already observe an increase in the induction that continued until 6 hours after DTT addition, when GFP levels reached a plateau (Figure 1B). It is important to mention that UPR activation probably starts before clustering can be observed and that there exists a lag time between Ire1 sensing and the increase in UPRE-regulated GFP due to the time it takes to transcribe, translate and fold the GFP. Hence Ire1-mCherry clustering and UPRE-GFP increase each have their spatio-temporal restrictions. However, as both assays identified 2 hours as the earliest time point in which a clear UPR activation by these reporters could be assayed, we chose this time point for our screen.
To identify proteins that affect Ire1 clustering dynamics, we used a library of deletions in all non-essential yeast genes (Giaever et al., 2002) and a library of hypomorphic alleles of all essential ones (Breslow et al., 2008). Using a method for automated mating, sporulation and selection of desired haploids, we tailored the library such that each strain expressed Ire1-mCherry (Cohen and Schuldiner, 2011; Tong et al., 2001) (Figure 1C). After exposure of the strains to DTT for 2 hours, we imaged the entire collection using a high content imaging platform (Breker et al., 2013) and manually inspected and curated all of the images taking into consideration the number, the intensity and the size of the clusters. We identified 154 strains in which Ire1-mCherry clustering was altered as compared to a control strain (for a full list of hits and their phenotypes see Supplementary Table S1). We organized the hits into two groups (Figure 1D): “Enhanced clustering” or “Reduced clustering”. The large number of hits exemplifies the complexity of regulating a homeostatic response. However, it also poses an experimental difficulty in differentiating direct from indirect effects.

Genes involved in iron homeostasis affect Ire1 localization

To assess whether an entire cellular process was over-represented in our data, we performed a GO term enrichment analysis. The analysis uncovered a strong enrichment for processes that are related to iron and heme (itself a major iron dependent process) (Figure 2A).
Indeed, there were multiple effectors of iron levels, distribution and homeostasis among the hits from our screen. For example, deletions of the iron transporters Mrs3 and Smf3 caused a dramatic reduction in Ire1-mCherry clustering (Figure 2B). Similarly, deletions in other genes that govern iron homeostasis, such as the iron permease Ftr1, the ferric reductases Fre1 and Fre2 and the iron-regulon transcription factors Aft1 and Aft2, all caused a decreased clustering phenotype (Figure 2B). The dependence on iron homeostasis to mount a full-blown UPR has not been previously identified, hence we embarked on verifying the suggested connection.

Iron levels affect dynamics of Ire1 clustering and UPR activation

Since deletion of genes that are important for iron homeostasis may dramatically alter the cellular wiring, we tested whether iron depletion or repletion itself induces the UPR. To this end, we first

visualized Ire1-mCherry following iron depletion and found no effect on the localization of Ire1-mCherry (Supplementary Figure 1A). Moreover, we found that neither iron depletion nor repletion had an impact on UPR induction as measured by the UPRE-GFP reporter (Supplementary Figure 1B). In further support of the notion that iron levels themselves do not impact the UPR, iron depletion or repletion in the absence of stress also did not affect the growth rate of yeast (Figure 3A). From these findings, we conclude that iron depletion or repletion does not, it itself, cause ER stress.

However, upon induction of ER stress, iron depleted cultures grew poorly, while growth rates improved at high iron concentrations (Figure 3B). This finding suggests that iron availability is a limiting factor for mounting an effective UPR. Accordingly, while the rate of accumulation of GFP from a UPRE-GFP reporter following stress was similar regardless of iron availability, the levels reached a plateau sooner at high vs. low iron concentrations, indicative of a more-timely resolution of the stress (Figure 4C). Indeed, iron depletion prevented Ire1-mCherry clustering under ER stress conditions, while high iron concentrations promoted Ire1-mCherry clustering with faster kinetics than in standard medium (Figure 4D and Supplementary Movies 1 and 2), which could explain why the UPR was more effective in resolving ER stress when iron abounded.

Most salient features of the *IRE1-HAC1/XBP1* signaling pathway have been conserved from yeast to man, including ER-stress induced clustering of Ire1/IRE1α (Li et al., 2010). To test whether iron levels feed into IRE1α signaling in humans as well, we employed HeLa cells in which IRE1α was ablated by CRISPR-Cas9 but was reconstituted with murine IRE1α-GFP expressed at near-endogenous levels. We visualized IRE1α-GFP expressing HeLa cells upon iron depletion (using the iron chelator Deferoxamine (DFO)) or upon iron repletion (using ferric ammonium citrate (FAC)), under basal or ER stress conditions, as elicited by tunicamycin (Tm). Indeed, the dependence of clustering on iron availability was conserved between yeast Ire1 and human IRE1α: iron depletion abolished IRE1α-GFP clustering in response to ER stress, whereas iron repletion led to more robust IRE1α-GFP clustering than in control media (Figure 3E, F)

Heme is a limiting factor for Ire1 clustering

Why is iron affecting Ire1 clustering? Because there is no indication that Ire1 is a metalloprotein, we hypothesized that iron levels may be a limiting factor for Ire1 clustering and activation in an indirect manner. Our GO term enrichment analysis pointed to heme biosynthesis as a central, iron-dependent, process that affects the UPR (Figure 2A). In that respect, it was noteworthy that among the hits from our screen were two genes, *ISA1* and *ISA2*, which relate to iron sulfur cluster (ISC) formation. Deletion of either gene impeded clustering of Ire1-mCherry (Figure 4A). ISCs serve as co-factors for a wide variety of enzymes, including those responsible for heme biosynthesis. Moreover, several hits from our screen represented ablations of genes encoding heme containing proteins or enzymes involved in heme biosynthesis. Specifically, we found that mutations in Aac1 and Pet9, the two heme-precursor importers into mitochondria, (Figure 4B) caused reduced clustering of Ire1-mCherry. Conversely, deletion of Pug1, a protein that facilitates heme export from the cell, dramatically enhanced Ire1-mCherry clustering (Figure 4B), which likewise supports the notion that Ire1 clustering propensity correlates with heme availability. Additional hits from our screen further implicated heme homeostasis as a key determinant in ER stress responsiveness of the Ire1 pathway, since deletions of the genes that encode enzymes that control heme biosynthesis in the mitochondria, Hem12, Hem13, Hem14 and Hem15, all caused a reduced clustering of Ire1-mCherry (Figure 4C).

Regulators of heme biosynthesis also affected Ire1 clustering. Rox1 represses Hem13 transcription when heme levels are elevated (Zhang and Hach, 1999; Zitomer and Lowry, 1992). Deletion of Rox1 thus leads to increased intracellular heme levels, and, accordingly, promoted Ire1-mCherry clustering (Figure 4D). The heme-activated transcriptional factor Hap1 translocates to the nucleus to drive Rox1 expression, but Ydj1 counteracts Hap1 activity by sequestering it in the cytosol (Lan et al., 2004). Hence, deletion of Ydj1 should lead to increased Rox1 levels and thereby to lowered heme biosynthesis. Indeed, Ire1-mCherry clustering was impeded when Ydj1 was ablated (Figure 4D). In summary, our findings demonstrate that heme availability is a limiting factor for Ire1's responsiveness to ER stress. Hence, while we do not show a causal and direct connection between iron levels and heme availability, it would be tempting to hypothesize that the requirement for iron in UPR activation is due to its essential role in heme biosynthesis

Why would heme have such an important role in UPR activation? To gain insight into this question, we mapped the overlap between all known heme containing proteins (Kaniak-Golik and Skoneczna, 2015), UPR targets (Travers et al., 2000) and the hits from our screen. Strikingly, we observed that iron repletion mechanisms are activated by the UPR as is the transcription of many heme biosynthetic enzymes. Hence there is cross-talk between iron/heme and ER homeostasis: iron/heme levels affect the UPR and the UPR promotes iron repletion and heme biosynthesis (Figure 4E). Importantly, we noticed that several hits from our screen were heme dependent enzymes, amongst them the ergosterol biosynthetic enzymes, Erg5 and Erg11 (Figure 4E). These results led us to hypothesize that the dependence on heme could be due to the essential role of heme in sterol biosynthesis.

Sterols biosynthesis affects Ire1 clustering

Sterol levels, and more generally, collective membrane properties such as fluidity, have previously been suggested to act as important modulators of ER stress signaling (Pineau et al., 2009; Promlek et al., 2011; Surma et al., 2013; Thibault et al., 2012; Volmer et al., 2013). Indeed, we have recently shown that such bi-layer properties are directly sensed by the unique trans-membrane region of Ire1 (Halbleib et al., 2017). We hence decided to follow sterol levels following induction of ER stress and found that there is a rapid and dramatic decrease in ER membrane sterol levels (Figure 5A, Supplementary Table S2). This drop of membrane sterols is remarkable, because previous work by others showed that membrane sterols are kept at a constant level under a wide variety of growth conditions (Klose et al., 2012). This suggests a strong requirement to upregulate sterol biosynthesis to support Ire1-mCherry cluster formation at later times following the stress.

In support of this was the fact that deletions of both heme containing ergosterol biosynthesis enzymes, Erg5 and Erg11, came up in our screen as preventing Ire1-mCherry clustering (Figure 5B) similar to the effect of iron or heme depletion. These findings led us to hypothesize that the ergosterol content in the membrane (either directly or indirectly) is an additional factor affecting Ire1 clustering and, thereby, UPR signaling. To support this notion, we first manually deleted three additional non-essential ergosterol biosynthesis enzymes (Figure 5C) and additionally created shut-down alleles for two essential ergosterol biosynthesis enzymes (Figure 5D). Regardless of the enzyme whose function we perturbed, we consistently ablated Ire1 clustering. Hence it is not the accumulation or reduction in any specific sterol species but rather a depletion of overall sterol levels that is the underlying cause for loss of clustering.

Moreover, loss of any non-essential ergosterol-pathway enzyme led to complete inability to survive even the mildest of ER stresses, such as that caused by inositol depletion (Cox et al., 1997; Lajoie et

al., 2012) (Figure 5E). This stresses the requirement for optimal de-novo ergosterol biosynthesis capacities to mount a functional homeostatic response.
However, genetic alterations to the ergosterol pathway cause many pleiotropic effects, making it hard to gauge whether the effects on Ire1 clustering are direct or indirect. To test the role of ergosterol more directly, we employed two ergosterol synthesis inhibitors working on different steps in the pathway: fluconazole (Erg11 inhibitor) and Terbinafine (Erg1 inhibitor). Treatment with either drug confirmed that under ER stress conditions Ire1-mCherry no longer clustered when ergosterol biosynthesis was inhibited (Figure 5F) and the UPR was not efficiently activated (Supplementary Figure 2).

A feedback loop exists between ER stress, iron levels and ergosterol biosynthesis
If iron is essential for mounting a full-blown UPR, then it stands to reason that the cell would regulate iron uptake when the UPR is induced. Indeed, we found that the major iron regulon inducer, the transcription factor Aft1 (Yamaguchi-Iwai, 2002), translocates to the nucleus following ER stress (Figure 6A). Moreover, some of the targets of Aft1 also came up as hits in the screen suggesting that their upregulation is required to sustain Ire1 clustering (Supplementary Table S3). Interestingly ablation of sterol biosynthesis concomitantly with the onset of ER stress suppressed Aft1 nuclear localization suggesting that Aft1 translocation to the nucleus is not a direct result of ER stress sensing but rather a secondary effect of upregulated ergosterol biosynthesis (Figure 6A). Taken together all of our above findings, while not directly showing a causal connection between iron, heme and ergosterol, suggest a testable model whereby unfolded protein stress, iron uptake/utilization, heme biosynthesis and ergosterol build-up are all interconnected through a feedback loop (Figure 6B).

Discussion
Our screen unveiled that Ire1 clustering is affected by ablation of a wide range of proteins among them those that play a role in chromatin remodeling, transcription, translation or mRNA stability. Apparently, a broad network of transcription and translation regulates fine-tuning of the UPR meriting further investigation.
Another striking observation from our screen is that a reduction of Ire1 clustering seems to be controlled by signaling cascades. Amongst our hits were Npr2, a regulator of the TOR pathway (Laxman et al., 2014), Sap155 a regulator of the Sit4 phosphatase (Luke et al., 1996), Reg1 a regulatory subunit of the Glc7 phosphatase (Tu and Carlson, 1995) and the protein kinase, Mck1 (Cherry et al., 2012). It is tempting to speculate that these factors could modulate the Ire1 behavior by altering its phosphorylation status, directly or indirectly. The notion that metabolic input may feed in to the phosphorylation status of Ire1 is not unprecedented: in hepatocytes, glucagon-induced Protein Kinase A (PKA) phosphorylates IRE1α, which then contributes to gluconeogenic transcription via a still poorly understood mechanism (Mao et al., 2011).
We specifically chose to focus on the strongest link that came up from the screen that was with iron/heme homeostasis. The model that emerged from our data poses that Ire1 clustering propensity and hence, the amplitude of Ire1 signaling, is dependent, at least in part, on sterol levels in the ER membrane. Since it is not clear at present whether this is direct or not we can only speculate that membrane bilayer packing or membrane reshaping have an effect on Ire1 clustering. This notion is in line with other reports, showing that desaturation of fatty acyl chains and ergosterol accumulation, which lead to similar membrane packing alterations, dramatically affect Ire1

activation (Surma et al., 2013; Volmer et al., 2013) and ER stress (Deguil et al., 2011; Feng et al., 2003; Gardner and Walter, 2011; Lajoie et al., 2012; Pineau et al., 2009). The transmembrane domain of Ire1, in fact, is unusual in length and sequence (Promlek et al., 2011) and we could recently show that it can directly sense and respond to altered lipid content (Halbleib et al., 2017). Our data, while not directly showing causality, enable us to put forward a working hypothesis. We suggest that in the absence of sufficient iron, ISC and heme biosynthesis is reduced, which, in turn, compromises synthesis of ergosterol/cholesterol, causing increased fluidity of the ER membrane and, as such, interfering with Ire1 clustering (Figure 6B). It remains to be elucidated whether Ire1 clustering goes hand in hand with membrane reorganization events and whether Ire1 clusters originate at pre-existing sites where the ER membrane composition is such that it can sustain clustering.

Our findings highlight that iron/heme availability are of such importance for mounting an efficient UPR that they themselves are controlled by UPR activation creating a feedback loop (Figure 6B). An involvement of heme in modulating the UPR has been reported before: reduced heme levels activate HRI (Heme-regulated inhibitor) in mammalian cells that in turn causes phosphorylation of eIF2α, triggering activation of the integrated stress response, which is also invoked by the PERK signaling branch of the UPR (Han et al., 2001). Our results now suggest a mechanism for this dependence – through membrane architecture alterations that are dependent on heme containing enzymes.

The insights that we have gained on the cross-talk between ER stress signaling and iron/heme homeostasis are interesting also in light of human pathogenesis. Enhanced IRE1α clustering and an increased amplitude of UPR signaling caused by iron repletion may well lie at the basis of the increased risk for patients that suffer from hemochromatosis (i.e. pathological iron overload) of developing type 2 diabetes (Simcox and McClain, 2013; Wang et al., 2015). The condition that emerges when ER stress signaling in pancreatic beta-cells is excessive, leading to their apoptotic death (Marciniak and Ron, 2006). In further support of how our model may explain the link between excess iron and the onset of diabetes, several lines of evidence indicate that boosting heme oxygenase-1 (HO-1) activity, which lowers heme levels, can alleviate diabetes (Abraham et al., 2008).

More broadly, our findings highlight that stress responses are orchestrated through integration of a variety of homeostatic pathways. They also uncover a role for mitochondria/ER cross talk in alleviating stress. In the absence of optimal mitochondrial activity, heme biosynthesis will be altered and the ER will not mount the maximal stress response – potentially leaving cellular resources for dealing with mitochondrial stress. Ire1 therefore emerges as a molecular hub that integrates multiple aspects of cell metabolism such that ER stress responses not only meet protein-folding demands, but are also in tune with the overall status of the cell.

Materials and Methods

Yeast strains, strain construction and culturing conditions

All strains in this study are based on the BY4741 laboratory strain (Brachmann et al., 1998). All information on strains, plasmids and primers can be found in Supplementary Table S4, S5 and S6. The libraries used were the yeast deletion library (Giaever et al., 2002) and the DAmP hypomorphic allele library (Breslow et al., 2008). the GFP-Aft1 was taken from the yeast seamless version of the SWAT-GFP library (Yofe et al., 2016).

For the lipidomics a BY4741 WT strain was grown from OD_{600} of~0.1 to 0.8 in the respective

medium and then treated for 1h with 2mM DTT.
For the majority of experiments yeast were grown in standard synthetic dextrose (SD) medium (6.7 g/L yeast nitrogen base with ammonium sulfate, 2% glucose and all necessary amino acids). For inositol depletion experiments yeast nitrogen base – inositol (USbiological) was used. Yeast nitrogen base without iron (Sunrise science products) was used for iron depletion/repletion experiments, and supplemented with the indicated concentrations of $FeCl_3$ (Sigma). For media for the microscopy screening yeast nitrogen base without Riboflavin was used (Formedium).
DTT (Sigma) was used at 2mM, Tunicamycin (Sigma) was used at 5µg/ml, Fluconazole (Sigma) was used at 3.3µg/ml, Terbinafine(Sigma) was used at 10µg/ml. Repression of the TET promoter for the yeast strains was performed using 15µg/ml Doxycycline for 11hours.

Yeast library preparation

To create the collection of haploid strains containing Ire1-mCherry on the background of all yeast mutants, an Ire1-mCherry expressing query strain was constructed on the basis of a synthetic genetic array (SGA) compatible strain, YMS721 (Papić et al., 2013). Using the SGA method (Cohen and Schuldiner, 2011; Tong and Boone, 2006) the Ire1-mCherry query strain was crossed with the libraries. To perform the SGA in high-density format we used a RoToR bench top colony arrayer (Singer Instruments). In short: mating was performed on rich medium plates, and selection for diploid cells was performed on SD-URA plates containing Geneticin (200µg/mL). Sporulation was induced by transferring cells to nitrogen starvation media plates for 7 days. Haploid cells containing the desired mutations were selected by transferring cells to SD-URA plates containing Geneticin (200µg/mL) alongside the toxic amino acid derivatives Canavanine and Thialysine (Sigma-Aldrich) to select against remaining diploids, and lacking Histidine to select for spores with an A mating type.

Automated high-throughput fluorescence microscopy

The collection was visualized using an automated microscopy setup as described previously (Breker et al., 2013). In short: cells were transferred from agar plates into 384-well polystyrene plates for growth in liquid media using the RoToR arrayer robot. Liquid cultures were grown in a LiCONiC incubator, overnight at 30°C in SD medium lacking uracil to select for yeast containing the plasmid encoding Ire1-mCherry. A JANUS liquid handler (PerkinElmer) connected to the incubator was used to dilute the strains to an OD_{600} of ~0.2 into plates containing SD + DTT. Plates were incubated at 30°C for 2 hours. The cultures in the plates were then transferred by the liquid handler into glass-bottom 384-well microscope plates (Matrical Bioscience) coated with Concanavalin A (Sigma-Aldrich). After 20 minutes, wells were washed twice with SD-Riboflavin complete medium to remove non-adherent cells and to obtain a cell monolayer. The plates were then transferred to the ScanR automated inverted fluorescent microscope system (Olympus) using a robotic swap arm (Hamilton). Images of cells in the 384-well plates were recorded in SD-Riboflavin complete medium at 24°C using a 60× air lens (NA 0.9) and with an ORCA-ER charge-coupled device camera (Hamamatsu). Images were acquired in the mCherry channel (excitation filter 572/35 nm, emission filter 632/60 nm).

Inositol depletion spot assay

For the inositol depletion assays, strains were grown overnight at 30°C in SD medium with the selection required for each strain. The cultures were dilute to an OD_{600} of ~0.4, 0.2, 0.1 and 0.05. 2µl of each dilution were placed on an SD plate and an SD-inositol plate. The plates were incubated for 24h at 30°C and imaged.

Microscopy of yeast strains

For manual microscopy of yeast strains we used the VisiScope Confocal Cell Explorer system, composed of a Zeiss Yokogawa spinning disk scanning unit (CSU-W1) coupled with an inverted Olympus microscope (IX83; ×60 oil objective; Excitation wavelength of 488 nm for GFP and 560 nm for mCherry). Images were taken by a connected PCO-Edge sCMOS camera controlled by VisView software. All the images were processed using Fiji (Schindelin et al., 2012), the contrast was corrected using the auto adjust function, the background was removed using 50pixels rolling ball. Poisson noise was removed using the PureDenoise Fiji add-on.

Ergosterol extraction for mass spectrometry

Mass spectrometry-based ergosterol analysis was performed by Lipotype GmbH (Dresden, Germany) as described (Ejsing et al., 2009; Klose et al., 2012). Ergosterols were extracted using a two-step chloroform/methanol procedure (Ejsing et al., 2009). Samples were spiked with the internal standard stigmastatrienol. After extraction, the organic phase was transferred to an infusion plate and dried in a speed vacuum concentrator. 1st step dry extract was re-suspended in 7.5 mM ammonium acetate in chloroform/methanol/propanol (1:2:4, V:V:V) and 2nd step dry extract in 33% ethanol solution of methylamine in chloroform/methanol (0.003:5:1; V:V:V). All liquid handling steps were performed using Hamilton Robotics STARlet robotic platform with the Anti Droplet Control feature for organic solvent pipetting.

MS data acquisition, analysis and post-processing of Ergosterol levels

Samples were analyzed by direct infusion on a QExactive mass spectrometer (Thermo Scientific) equipped with a TriVersa NanoMate ion source (Advion Biosciences). Samples were analyzed in both positive and negative ion modes with a resolution of Rm/z=200=280000 for MS. MS only was used to monitor ergosterol as protonated ion of an acetylated derivative(Liebisch et al., 2006). Data were analyzed with in-house developed lipid identification software based on LipidXplorer (Herzog et al., 2011; Herzog et al., 2012). Data post-processing and normalization were performed using an in-house developed data management system. Only lipid identifications with a signal-to-noise ratio >5, and a signal intensity 5-fold higher than in corresponding blank samples were considered for further data analysis.

Mammalian cell culture and growth conditions

HeLa cells were genotyped by PCR single locus technology to be HeLa S3. Ire1-KO cells were negatively tested for mycoplasma contamination on Nov 10, 2016 by PCR, on over weekend conditioned media, using the following primers:
myc Fw: ACTCCTACGGGAGGCAGCAGT
myc Rv: TGCACCATCTGTCACTCTGTTAACCTC
Cells were grown in Dulbecco's Modified Essential Medium (DMEM) GlutaMAX (Gibco-Life Technologies) supplemented with 5% Tet-System approved Fetal Bovine Serum (ClonTech), 10nM Doxycycline, 100 U/ml penicillin and 100 µg/ml streptomycin (Pen-Strep, Lonza BioWhittaker). Cells were cultured at 37°C in humidified 5% CO2 incubator and passaged twice a week. Cells

between 80% and 100% confluence were washed with PBS without Ca^{2+} and Mg^{2+} (DPBS) to get rid of both medium and dead cells and detached using Trypsin-EDTA (Gibco-Life Technologies). After detachment cells were centrifuged, re-suspended in medium and plated on a new plate. All cell lines used in this study were derived from HeLa cells that were modified by lentiviral infection to express the transgene of interest under inducible promoters. Production of lentiviral vectors was performed as previously described (Dull et al., 1998).
Iron depletion was obtained by addition of deferoxamine (DFO; Biofutura Pharma, Milan, Italy). Ferric ammonium citrate (FAC; Sigma-Aldrich) was used for iron loading experiments. Cells were incubated with 100 µM freshly prepared DFO or 300µM of FAC overnight and then treated with Tunicamycin 10µg/ml for 4 hours.

Generation of IRE1-KO and reconstituted TetON-mIRE1α-GFP HeLa cells
Using CRISPR/Cas9 methodology, we knocked out IRE1α in HeLa cells, resulting in an IRE1α-KO clonal cell line. The CRISPR strategy involved the creation of an indent and a subsequent frameshift at the level of the first exon (target sequence TCTTGCTTCCAAGCGTATACAGG). Knock-out clones were verified by western blot and by functional assays (i.e.: absence of XBP1 splicing upon ER stress). By lentiviral transduction we reconstituted IRE1α-KO-TetON cells by delivery of a cassette of green fluorescent protein-tagged murine IRE1α (IRE1α-GFP) under control of a "tight" Tet responsive element (Clontech), yielding clonal TetON-IRE1α-GFP cells. The GFP-tag was introduced into the juxtamembrane cytosolic linker domain of IRE1α, where such tagging had been shown before to not interfere with function of human IRE1α (Li et al., 2010b) or yeast Ire1 (Aragón et al., 2009). As expected, murine IRE1α-GFP clustered upon Tm treatment, similar to human IRE1α-GFP and yeast Ire1-GFP.

Microscopy of mammalian cell cultures
HeLa cells were grown on coverslips in 12-multiwell plates and fixed in 4% paraformaldehyde for 15 min at RT and washed in PBS. Nuclei were stained with DAPI diluted in PBS for 10 min at room temperature in the dark. After washing in PBS coverslips were mounted on microscope glass slides with Mowiol. Light microscopy images were acquired at the UltraView spinning disc confocal microscope operated by Volocity software (PerkinElmer). A 63x objective was used. GFP was excited with the 488 nm laser line.

Image analysis
To segment and calculate the area of the puncta in the mammalian cells we used *ilastik* (Sommer et al., 2011).

Calculating induction of the UPR using the UPRE-GFP reporter
Fold UPR activation was calculated in the following way:

$$fold\ UPR\ activation = \left(\frac{GFP_{final}}{OD_{600_{final}}}\right) - \left(\frac{GFP_{initial}}{OD_{600_{initial}}}\right)$$

Enrichment Analysis
Enrichment analysis for screen hits was performed by GOrilla analysis algorithm (Eden et al., 2007; Eden et al., 2009) .

Acknowledgements

We thank Blanche Schwappach and Alessandro Campanella for helpful discussions and protocols. We thank Michal Eisenberg-Bord, Einat Zalckvar and Nadav Shai for critical reading of the manuscript. We thank Idan Frumkin for the YMS1327 and YMS1328 strains. We thank Bernhard Gentner for help with lentiviral vector design and Andrew Basett for design of the sgRNA for deletion of IRE1α by CRISPR/Cas9. We thank Dr. Diego Alignani from the Flow Cytometry Unit at CIMA for providing technical advice in flow cytometry studies.

This work was partially supported by a Junior Fellow award from the Simons Foundation to MB. This work was performed through support of the DFG SFB1190 grant *Compartmental Gates and Contact Sites* to MS and a Volkswagen stiftung grant 93091 to MS and RE. MS is an Incumbent of the Dr. Gilbert Omenn and Martha Darling Professorial Chair in Molecular Genetics. EvA acknowledges financial support by the Armenise-Harvard foundation, Associazione Italiana per la ricerca sul Cancro (MFAG13584) and Ministero della Salute (RF-2011-02352852). TA acknowledges financial support by grants SAF2010-19239 and BFU2013-48703-P from the Spanish Ministry of Economy and Competitiveness TA was supported by a Ramon y Cajal contract from the Spanish Ministry of Science and Innovation, and from I3 program of the Spanish Ministry of Economy and Competitiveness. PW is an Investigator of the Howard Hughes Medical Institute.

References

Abraham, N. G., Tsenovoy, P. L., McClung, J. and Drummond, G. S. (2008). Heme oxygenase: a target gene for anti-diabetic and obesity. *Curr. Pharm. Des.* **14**, 412–21.

Aragón, T., van Anken, E., Pincus, D., Serafimova, I. M., Korennykh, A. V, Rubio, C. A. and Walter, P. (2009). Messenger RNA targeting to endoplasmic reticulum stress signalling sites. *Nature* **457**, 736–40.

Breker, M., Gymrek, M. and Schuldiner, M. (2013). A novel single-cell screening platform reveals proteome plasticity during yeast stress responses. *J. Cell Biol.* **200**, 839–50.

Breslow, D. K., Cameron, D. M., Collins, S. R., Schuldiner, M., Jacob, S.-O., Newman, H. W., Braun, S., Madhani, H. D., Krogan, N. J. and Weissman, J. S. (2008). A comprehensive strategy enabling high-resolution functional analysis of the yeast genome. *Nat. Methods* **5**, 711–718.

Cherry, J. M., Hong, E. L., Amundsen, C., Balakrishnan, R., Binkley, G., Chan, E. T., Christie, K. R., Costanzo, M. C., Dwight, S. S., Engel, S. R., et al. (2012). Saccharomyces Genome Database: the genomics resource of budding yeast. *Nucleic Acids Res.* **40**, D700-5.

Cohen, Y. and Schuldiner, M. (2011). Advanced methods for high-throughput microscopy screening of genetically modified yeast libraries. *Methods Mol. Biol.* **781**, 127–159.

Cox, J. S. and Walter, P. (1996). A novel mechanism for regulating activity of a transcription factor that controls the unfolded protein response. *Cell* **87**, 391–404.

Cox, J. S., Shamu, C. E. and Walter, P. (1993). Transcriptional induction of genes encoding endoplasmic reticulum resident proteins requires a transmembrane protein kinase. *Cell* **73**, 1197–206.

Cox, J. S., Chapman, R. E. and Walter, P. (1997). The unfolded protein response coordinates the production of endoplasmic reticulum protein and endoplasmic reticulum membrane. *Mol. Biol. Cell* **8**, 1805–1814.

Deguil, J., Pineau, L., Rowland Snyder, E. C., Dupont, S., Beney, L., Gil, A., Frapper, G. and Ferreira, T. (2011). Modulation of lipid-induced ER stress by fatty acid shape. *Traffic* **12**, 349–62.

Dull, T., Zufferey, R., Kelly, M., Mandel, R. J., Nguyen, M., Trono, D. and Naldini, L. (1998).

A Third-Generation Lentivirus Vector with a Conditional Packaging System. *J. Virol.* **72**, 8463–8471.

Eden, E., Lipson, D., Yogev, S. and Yakhini, Z. (2007). Discovering Motifs in Ranked Lists of DNA Sequences. *PLoS Comput. Biol.* **3**, e39.

Eden, E., Navon, R., Steinfeld, I., Lipson, D. and Yakhini, Z. (2009). GOrilla: a tool for discovery and visualization of enriched GO terms in ranked gene lists. *BMC Bioinformatics* **10**, 48.

Ejsing, C. S., Sampaio, J. L., Surendranath, V., Duchoslav, E., Ekroos, K., Klemm, R. W., Simons, K. and Shevchenko, A. (2009). Global analysis of the yeast lipidome by quantitative shotgun mass spectrometry. *Proc. Natl. Acad. Sci.* **106**, 2136–2141.

Feng, B., Yao, P. M., Li, Y., Devlin, C. M., Zhang, D., Harding, H. P., Sweeney, M., Rong, J. X., Kuriakose, G., Fisher, E. A., et al. (2003). The endoplasmic reticulum is the site of cholesterol-induced cytotoxicity in macrophages. *Nat. Cell Biol.* **5**, 781–92.

Gardner, B. M. and Walter, P. (2011). Unfolded proteins are Ire1-activating ligands that directly induce the unfolded protein response. *Science* **333**, 1891–4.

Gardner, B. M., Pincus, D., Gotthardt, K., Gallagher, C. M. and Walter, P. (2013). Endoplasmic reticulum stress sensing in the unfolded protein response. *Cold Spring Harb. Perspect. Biol.* **5**, a013169.

Giaever, G., Chu, A. M., Ni, L., Connelly, C., Riles, L., Véronneau, S., Dow, S., Lucau-Danila, A., Anderson, K., André, B., et al. (2002). Functional profiling of the Saccharomyces cerevisiae genome. *Nature* **418**, 387–391.

Halbleib, K., Pesek, K., Covino, R., Hofbauer, H. F., Wunnicke, D., Hanelt, I., Hummer, G. and Ernst, R. (2017). Activation of the Unfolded Protein Response by Lipid Bilayer Stress. *Mol. Cell*.

Han, A. P., Yu, C., Lu, L., Fujiwara, Y., Browne, C., Chin, G., Fleming, M., Leboulch, P., Orkin, S. H. and Chen, J. J. (2001). Heme-regulated eIF2alpha kinase (HRI) is required for translational regulation and survival of erythroid precursors in iron deficiency. *EMBO J.* **20**, 6909–18.

Herzog, R., Schwudke, D., Schuhmann, K., Sampaio, J. L., Bornstein, S. R., Schroeder, M. and Shevchenko, A. (2011). A novel informatics concept for high-throughput shotgun lipidomics based on the molecular fragmentation query language. *Genome Biol.* **12**, R8.

Herzog, R., Schuhmann, K., Schwudke, D., Sampaio, J. L., Bornstein, S. R., Schroeder, M. and Shevchenko, A. (2012). Lipidxplorer: A software for consensual cross-platform lipidomics. *PLoS One* **7**, 15–20.

Kaniak-Golik, A. and Skoneczna, A. (2015). Mitochondria-nucleus network for genome stability. *Free Radic. Biol. Med.* **82**, 73–104.

Kimata, Y., Ishiwata-Kimata, Y., Ito, T., Hirata, A., Suzuki, T., Oikawa, D., Takeuchi, M. and Kohno, K. (2007). Two regulatory steps of ER-stress sensor Ire1 involving its cluster formation and interaction with unfolded proteins. *J. Cell Biol.* **179**, 75–86.

Klose, C., Surma, M. A., Gerl, M. J., Meyenhofer, F., Shevchenko, A. and Simons, K. (2012). Flexibility of a eukaryotic lipidome - insights from yeast lipidomics. *PLoS One* **7**,.

Lajoie, P., Moir, R. D., Willis, I. M. and Snapp, E. L. (2012). Kar2p availability defines distinct forms of endoplasmic reticulum stress in living cells. *Mol. Biol. Cell* **23**, 955–64.

Lan, C., Lee, H. C., Tang, S. and Zhang, L. (2004). A novel mode of chaperone action: Heme activation of Hap1 by enhanced association of Hsp90 with the repressed Hsp70-Hap1 complex. *J. Biol. Chem.* **279**, 27607–27612.

Laxman, S., Sutter, B. M., Shi, L. and Tu, B. P. (2014). Npr2 inhibits TORC1 to prevent inappropriate utilization of glutamine for biosynthesis of nitrogen-containing metabolites. *Sci. Signal.* **7**, ra120-ra120.

Li, H., Korennykh, a V, Behrman, S. L. and Walter, P. (2010). Mammalian endoplasmic reticulum stress sensor IRE1 signals by dynamic clustering. *Proc Natl Acad Sci U S A* **107**, 16113–16118.

Liebisch, G., Binder, M., Schifferer, R., Langmann, T., Schulz, B. and Schmitz, G. (2006). High throughput quantification of cholesterol and cholesteryl ester by electrospray ionization tandem mass spectrometry (ESI-MS/MS). *Biochim. Biophys. Acta - Mol. Cell Biol. Lipids* **1761**, 121–128.

Luke, M. M., Della Seta, F., Di Como, C. J., Sugimoto, H., Kobayashi, R. and Arndt, K. T. (1996). The SAP, a new family of proteins, associate and function positively with the SIT4 phosphatase. *Mol. Cell. Biol.* **16**, 2744–55.

Mao, T., Shao, M., Qiu, Y., Huang, J., Zhang, Y., Song, B., Wang, Q., Jiang, L., Liu, Y., Han, J.-D. J., et al. (2011). PKA phosphorylation couples hepatic inositol-requiring enzyme 1 to glucagon signaling in glucose metabolism. *Proc. Natl. Acad. Sci.* **108**, 15852–15857.

Marciniak, S. J. and Ron, D. (2006). Endoplasmic Reticulum Stress Signaling in Disease. *Physiol. Rev.* **86**, 1133–1149.

McClellan, A. J., Endres, J. B., Vogel, J. P., Palazzi, D., Rose, M. D. and Brodsky, J. L. (1998). Specific molecular chaperone interactions and an ATP-dependent conformational change are required during posttranslational protein translocation into the yeast ER. *Mol. Biol. Cell* **9**, 3533–45.

Mori, K., Ma, W., Gething, M. J. and Sambrook, J. (1993). A transmembrane protein with a cdc2+/CDC28-related kinase activity is required for signaling from the ER to the nucleus. *Cell* **74**, 743–56.

Okamura, K., Kimata, Y., Higashio, H., Tsuru, a and Kohno, K. (2000). Dissociation of Kar2p/BiP from an ER sensory molecule, Ire1p, triggers the unfolded protein response in yeast. *Biochem. Biophys. Res. Commun.* **279**, 445–50.

Papić, D., Elbaz-Alon, Y., Koerdt, S. N., Leopold, K., Worm, D., Jung, M., Schuldiner, M. and Rapaport, D. (2013). The role of Djp1 in import of the mitochondrial protein Mim1 demonstrates specificity between a cochaperone and its substrate protein. *Mol. Cell. Biol.* **33**, 4083–4094.

Pineau, L., Colas, J., Dupont, S., Beney, L., Fleurat-Lessard, P., Berjeaud, J. M., Berg??s, T. and Ferreira, T. (2009). Lipid-induced ER stress: Synergistic effects of sterols and saturated fatty acids. *Traffic* **10**, 673–690.

Promlek, T., Ishiwata-Kimata, Y., Shido, M., Sakuramoto, M., Kohno, K. and Kimata, Y. (2011). Membrane aberrancy and unfolded proteins activate the endoplasmic reticulum stress sensor Ire1 in different ways. *Mol. Biol. Cell* **22**, 3520–3532.

Schindelin, J., Arganda-Carreras, I., Frise, E., Kaynig, V., Longair, M., Pietzsch, T., Preibisch, S., Rueden, C., Saalfeld, S., Schmid, B., et al. (2012). Fiji: an open-source platform for biological-image analysis. *Nat. Methods* **9**, 676–682.

Shamu, C. E. and Walter, P. (1996). Oligomerization and phosphorylation of the Ire1p kinase during intracellular signaling from the endoplasmic reticulum to the nucleus. *EMBO J.* **15**, 3028–39.

Simcox, J. A. and McClain, D. A. (2013). Iron and Diabetes Risk. *Cell Metab.* **17**, 329–341.

Sommer, C., Straehle, C., Kothe, U. and Hamprecht, F. A. (2011). Ilastik: Interactive learning and segmentation toolkit. In *2011 IEEE International Symposium on Biomedical Imaging: From Nano to Macro*, pp. 230–233. IEEE.

Surma, M. A., Klose, C., Peng, D., Shales, M., Mrejen, C., Stefanko, A., Braberg, H., Gordon, D. E., Vorkel, D., Ejsing, C. S., et al. (2013). A lipid E-MAP identifies Ubx2 as a critical regulator of lipid saturation and lipid bilayer stress. *Mol. Cell* **51**, 519–30.

Thibault, G., Shui, G., Kim, W., McAlister, G. C., Ismail, N., Gygi, S. P., Wenk, M. R. and Ng, D. T. W. (2012). The membrane stress response buffers lethal effects of lipid disequilibrium by reprogramming the protein homeostasis network. *Mol. Cell* **48**, 16–27.

Tirasophon, W., Welihinda, A. A. and Kaufman, R. J. (1998). A stress response pathway from the endoplasmic reticulum to the nucleus requires a novel bifunctional protein kinase/endoribonuclease (Ire1p) in mammalian cells. *Genes Dev.* **12**, 1812–24.

Todd-Corlett, A., Jones, E., Seghers, C. and Gething, M. J. (2007). Lobe IB of the ATPase

Domain of Kar2p/BiP Interacts with Ire1p to Negatively Regulate the Unfolded Protein Response in Saccharomyces cerevisiae. *J. Mol. Biol.* **367**, 770–787.

Tong, A. H. Y. and Boone, C. (2006). Synthetic genetic array analysis in Saccharomyces cerevisiae. *Methods Mol. Biol.* **313**, 171–192.

Tong, A. H., Evangelista, M., Parsons, A. B., Xu, H., Bader, G. D., Pagé, N., Robinson, M., Raghibizadeh, S., Hogue, C. W., Bussey, H., et al. (2001). Systematic genetic analysis with ordered arrays of yeast deletion mutants. *Science* **294**, 2364–8.

Travers, K. J., Patil, C. K., Wodicka, L., Lockhart, D. J., Weissman, J. S. and Walter, P. (2000). Functional and genomic analyses reveal an essential coordination between the unfolded protein response and ER-associated degradation. *Cell* **101**, 249–258.

Tu, J. and Carlson, M. (1995). REG1 binds to protein phosphatase type 1 and regulates glucose repression in Saccharomyces cerevisiae. *EMBO J.* **14**, 5939–46.

van Anken, E., Pincus, D., Coyle, S., Aragón, T., Osman, C., Lari, F., Gómez Puerta, S., Korennykh, A. V and Walter, P. (2014). Specificity in endoplasmic reticulum-stress signaling in yeast entails a step-wise engagement of HAC1 mRNA to clusters of the stress sensor Ire1. *Elife* **3**, e05031.

Volmer, R. and Ron, D. (2015). Lipid-dependent regulation of the unfolded protein response. *Curr. Opin. Cell Biol.* **33**, 67–73.

Volmer, R., van der Ploeg, K. and Ron, D. (2013). Membrane lipid saturation activates endoplasmic reticulum unfolded protein response transducers through their transmembrane domains. *Proc. Natl. Acad. Sci. U. S. A.* **110**, 4628–4633.

Walter, P. and Ron, D. (2011). The Unfolded Protein Response: From Stress Pathway to Homeostatic Regulation. *Science (80-.).* **334**, 1081–1086.

Wang, X., Fang, X. and Wang, F. (2015). Pleiotropic actions of iron balance in diabetes mellitus. *Rev. Endocr. Metab. Disord.* **16**, 15–23.

Yamaguchi-Iwai, Y. (2002). Subcellular Localization of Aft1 Transcription Factor Responds to Iron Status in Saccharomyces cerevisiae. *J. Biol. Chem.* **277**, 18914–18918.

Yofe, I., Weill, U., Meurer, M., Chuartzman, S., Zalckvar, E., Goldman, O., Ben-Dor, S., Schütze, C., Wiedemann, N., Knop, M., et al. (2016). One library to make them all: streamlining the creation of yeast libraries via a SWAp-Tag strategy. *Nat. Methods* **13**, 371–378.

Yoshida, H., Haze, K., Yanagi, H., Yura, T. and Mori, K. (1998). Identification of the cis-acting endoplasmic reticulum stress response element responsible for transcriptional induction of mammalian glucose-regulated proteins. Involvement of basic leucine zipper transcription factors. *J. Biol. Chem.* **273**, 33741–9.

Yoshida, H., Matsui, T., Yamamoto, A., Okada, T. and Mori, K. (2001). XBP1 mRNA is induced by ATF6 and spliced by IRE1 in response to ER stress to produce a highly active transcription factor. *Cell* **107**, 881–891.

Zhang, L. and Hach, A. (1999). Molecular mechanism of heme signaling in yeast: The transcriptional activator Hap1 serves as the key mediator. *Cell. Mol. Life Sci.* **56**, 415–426.

Zitomer, R. S. and Lowry, C. V (1992). Regulation of gene expression by oxygen in Saccharomyces cerevisiae. *Microbiol. Rev.* **56**, 1–11.

Figure 1: A systematic high content screen reveals effectors of Ire1 clustering
A) Ire1-mCherry was visualized over time following induction of the UPR by 2mM DTT and shows clustering as expected. Scale bar represents 5 μm.
B) UPR activity was measured over time using a UPRE-GFP reporter following induction of UPR by 2mM DTT. UPR activity increases until an activation plateau is reached.
C) Work flow for systematic screen to uncover Ire1-mCherry clustering effectors.
D) Hits from the Ire1-mCherry screen were divided into two phenotypic groups. Scale bar represents 5 μm.

Figure 2: Iron homeostasis affects Ire1-mCherry clustering
A) GO-term enrichment of the hits in the screen based on the GOrilla analysis website. The table shows the ten highest enriched categories excluding redundant GO-terms
B) Deletion of several iron homeostasis genes disrupts Ire1-mCherry clustering following ER (2mM DTT) (images from original screen). Scale bar represents 5 μm.

Figure 3: Iron is essential for mounting a productive UPR
A) Iron depletion or repletion does not affect yeast growth under non-ER stress conditions as assayed by the change of O.D at 600nm per hour using a plate reader.
B) Iron repletion is essential to enable robust yeast growth during ER stress (2mM DTT) as assayed by the change of O.D at 600nm per hour using a plate reader.
C) The presence of iron enables mounting a more effective UPR response as can be seen by measuring the UPRE-GFP reporter over time under various iron repletion or depletion conditions following ER stress (2mM DTT).
D) Ire1-mCherry clustering following induction of ER stress (2mM DTT) is affected by the amount of iron in the medium. **$p<0.01$. Scale bar represents 5 μm.
E) Iron affects Ire1 clustering in mammalian HeLa cells treated with 10μg/ml Tunicamycin (TM). While iron depletion (100μM DFO) disrupts Ire1-GFP clustering, iron repletion (300μM FAC) enhances it. Bottom row is a magnification of the TM treated cells. Scale bar represents 10 μm.
F) Quantification of (E).

Figure 4: Iron sulfur cluster and heme biosynthesis are essential for Ire1-mCherry clustering
A) Deletion of the Iron Sulfur Cluster (ISC) biosynthesis proteins, *Δisa1* and *Δisa2* abrogates Ire1-mCherry clustering following stress (images from original screen). Scale bar represents 5 μm.
B) Reducing heme afflux *(*Δ*acc1*, *pet9-DAmP*) disrupts Ire1-mCherry clustering following stress, while reducing heme efflux *(*Δ*pug1*) enhances it (images from original screen). Scale bar represents 5 μm.
C) Mutations of the enzymes required for the last steps of the heme biosynthesis pathway disrupt Ire1-mCherry clustering following stress (images from original screen). Scale bar represents 5 μm.
D) Deletion of Ydj1, the positive regulator of the heme specific transcription factor *HAP1,* disrupts Ire1-mCherry clustering following stress, while deletion of the *HAP1* negative regulator, Rox1, enhances it (images from original screen). Scale bar represents 5 μm.
E) Venn diagram overlaying heme containing proteins, UPR upregulated genes, and Ire1 clustering effectors from the screen (Only the major GO term-enrichments are shown for each group). The diagram highlights a potential role for ergosterol biosynthesis (a-hypomorphic allele, b-not in the screen).

Figure 5: Ergosterol biosynthesis affects Ire1-mCherry clustering
A) ER stress causes a rapid and significant decrease in overall ergosterol levels. Analysis of the ergosterol content in shown in unstressed cells and following 2mM DTT treatment for 1h. *$p<0.05$
B) Deletions of the heme containing ergosterol biosynthesis pathway enzymes, Erg5 and Erg11, disrupt Ire1-mCherry clustering following ER stress (images from original screen). Scale bar represents 5 μm.

C) Deletions of the non-essential ergosterol biosynthesis pathway enzymes, Erg2, Erg3 and Erg6, disrupt Ire1-mCherry clustering following ER stress (2mM DTT). Scale bar represents 5 μm.
D) Repressing the expression of two essential ergosterol biosynthesis pathway enzymes: Erg12 and Erg25 using a TetOFF promotor repressed by doxycycline disrupts Ire1-mCherry clustering following ER stress (2mM DTT). Scale bar represents 5 μm.
E) Deletion strains of the non-essential components of the ergosterol biosynthesis pathway cannot grow even in mild ER stress conditions caused by removal of inositol from the medium.
F) Short term inhibition of ergosterol biosynthesis using two different inhibitors (Fluconazole 20μg/ml or Terbinafine 10μg/ml) disrupts Ire1-mCherry clustering following UPR induction (2mM DTT). Scale bar represents 5 μm.

Figure 6: Suggested crosstalk between the UPR, heme and iron homeostatic machinery
A) GFP-Aft1 re-localizes to the nucleus under unfolded protein stress, as induced by either 2mM DTT, 5μg/ml tunicamycin or 24 hours growth in inositol depletion media. The nuclear accumulation is inhibited by lowering ergosterol biosynthesis using ergosterol biosynthesis inhibitors (Fluconazole 20μg/ml or Terbinafine 10μg/ml). Scale bar represents 5 μm.
B) A schematic for a hypothetical feedback loop suggested for the heme and iron crosstalk with ergosterol biosynthesis and the UPR

Cohen *et al*, Figure 1

A

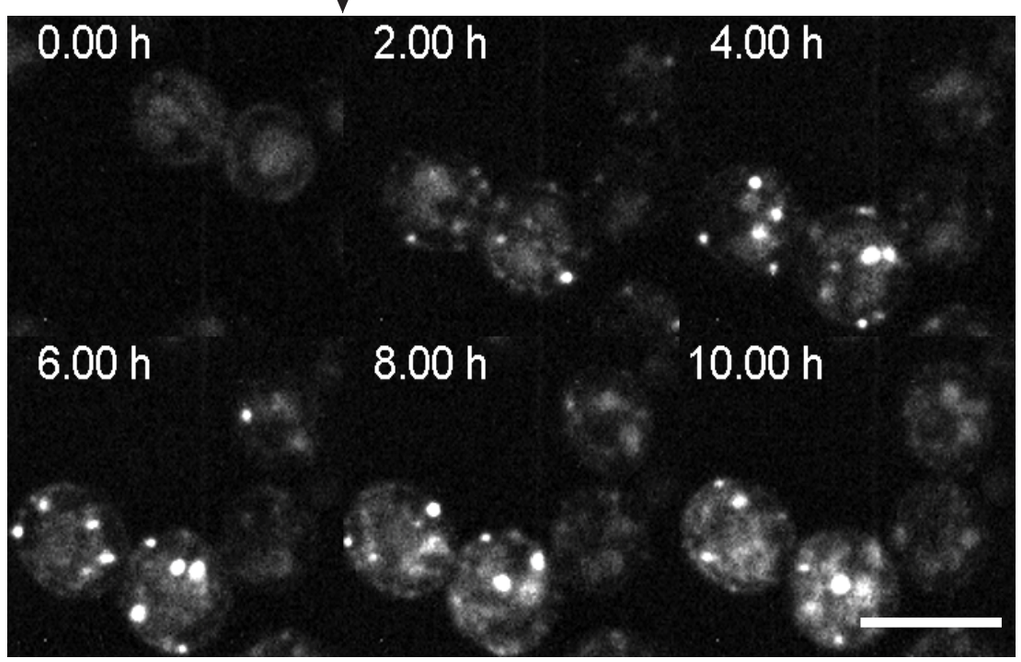

B

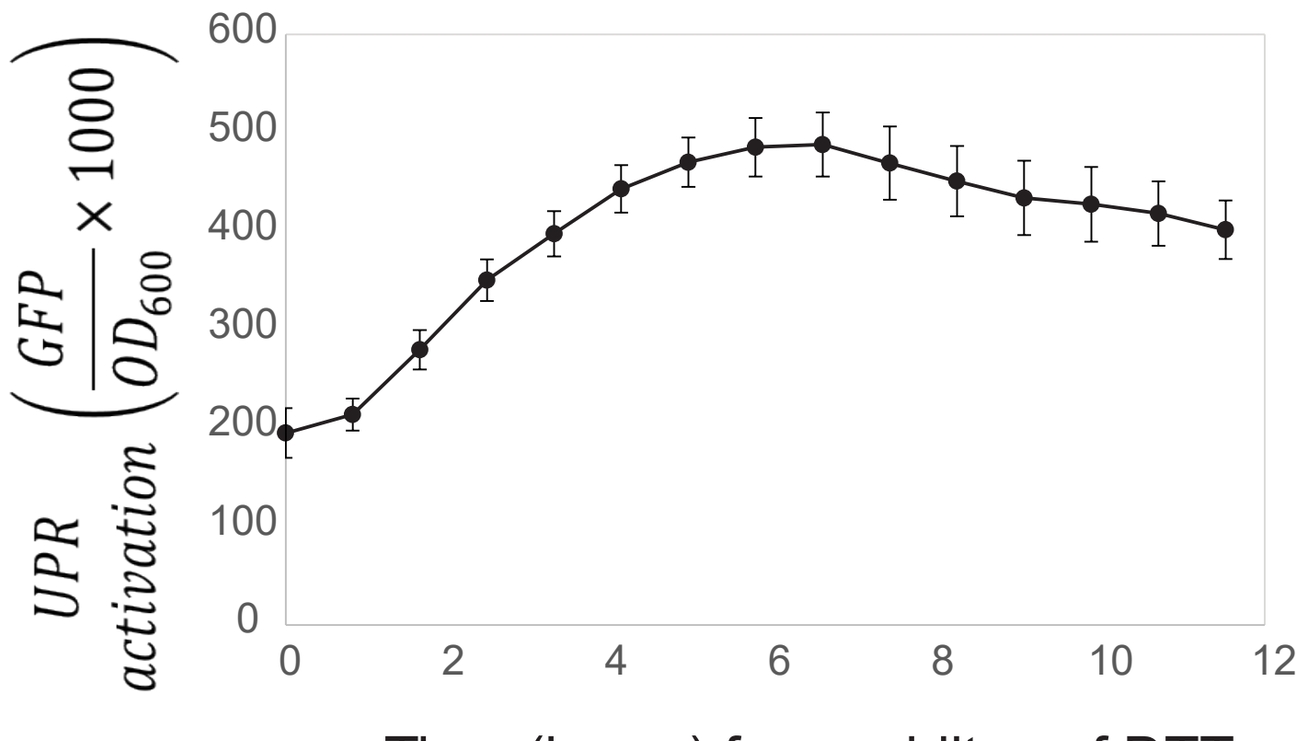

C

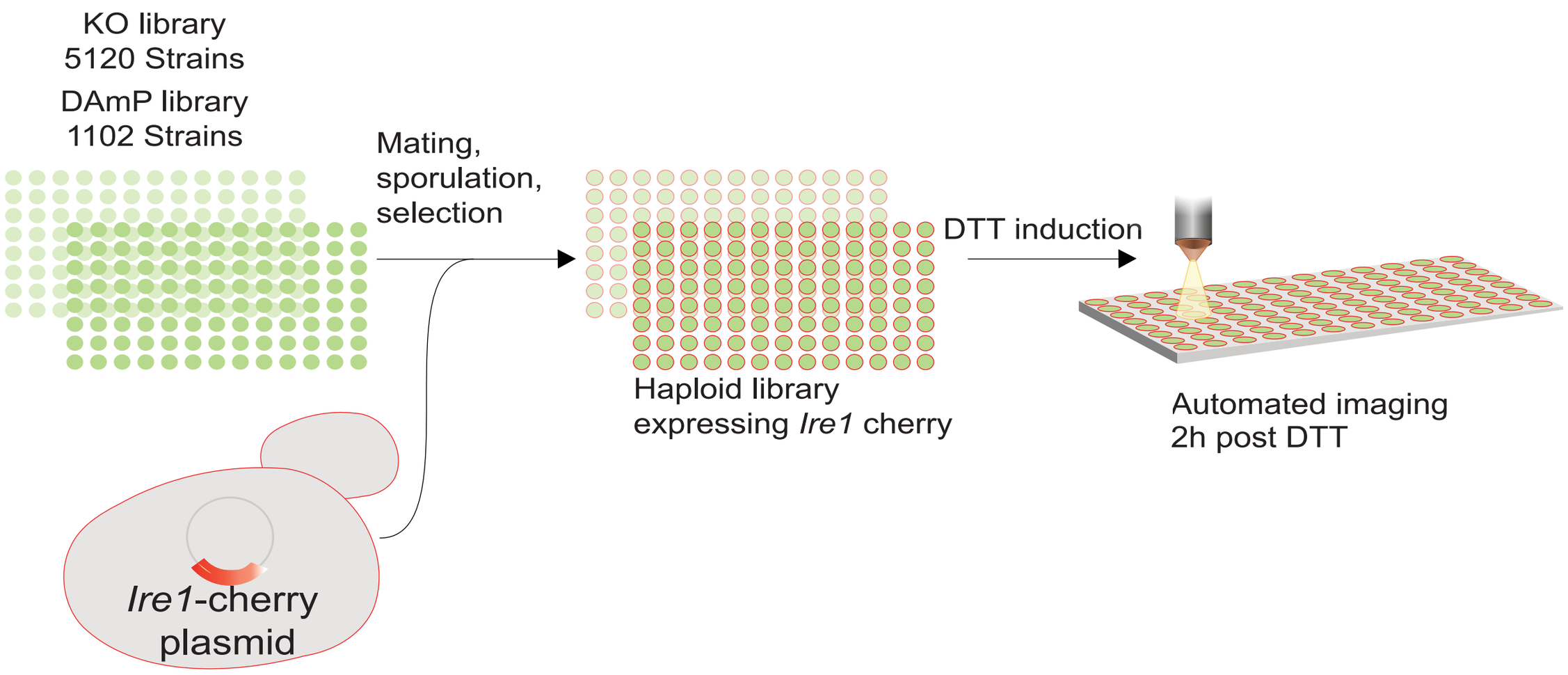

D

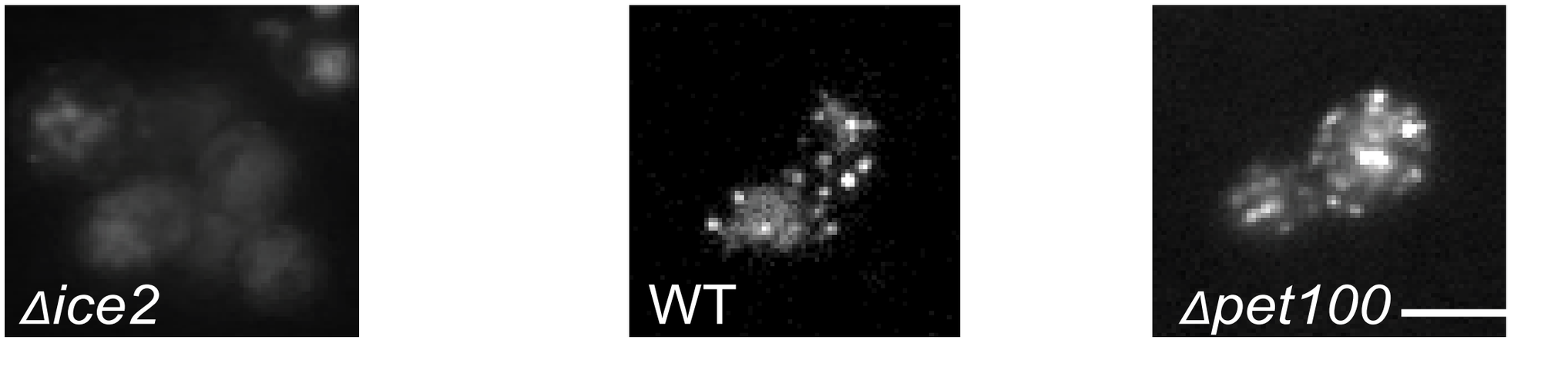

A

GO term	Description	P-value	FDR q-value	Enrichment
GO:0010106	**cellular response to iron ion starvation**	**6.63E-04**	**5.45E-02**	**38.71**
GO:0033217	**regulation of transcription from RNA polymerase II promoter in response to iron ion starvation**	**6.63E-04**	**5.36E-02**	**38.71**
GO:0015886	**heme transport**	**1.63E-04**	**1.69E-02**	**23.22**
GO:0097034	mitochondrial respiratory chain complex IV biogenesis	1.18E-12	6.00E-09	16.59
GO:0070129	regulation of mitochondrial translation	1.73E-06	3.26E-04	14.52
GO:0006783	**heme biosynthetic process**	**5.16E-05**	**7.52E-03**	**11.38**
GO:0006779	**porphyrin-containing compound biosynthetic process**	**5.16E-05**	**7.31E-03**	**11.38**
GO:0033014	**tetrapyrrole biosynthetic process**	**5.16E-05**	**7.11E-03**	**11.38**
GO:0006986	response to unfolded protein	3.49E-04	3.02E-02	11.06
GO:0006778	**porphyrin-containing compound metabolic process**	**7.00E-05**	**8.70E-03**	**10.75**

B

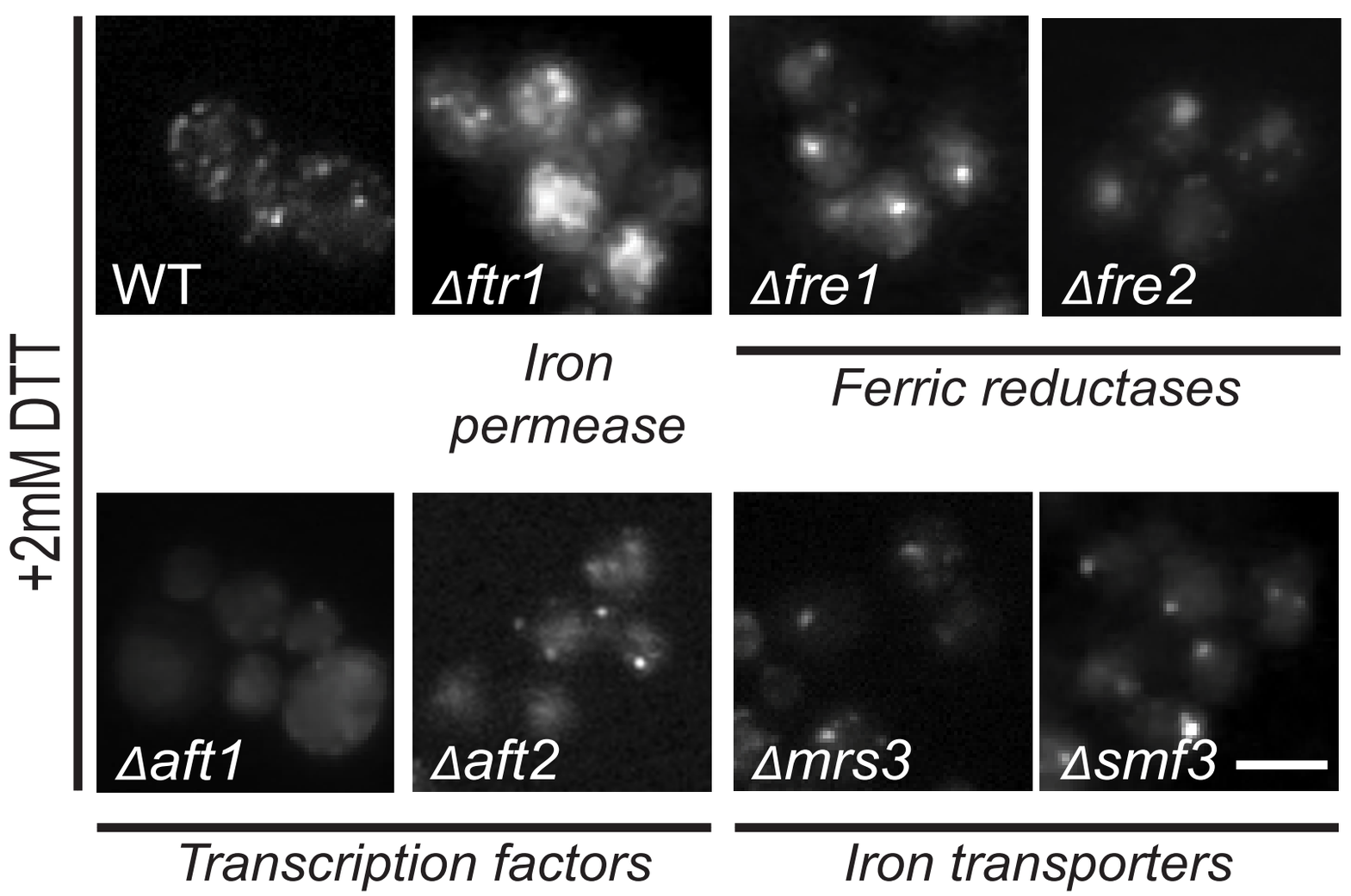

Cohen *et al*, Figure 3

A

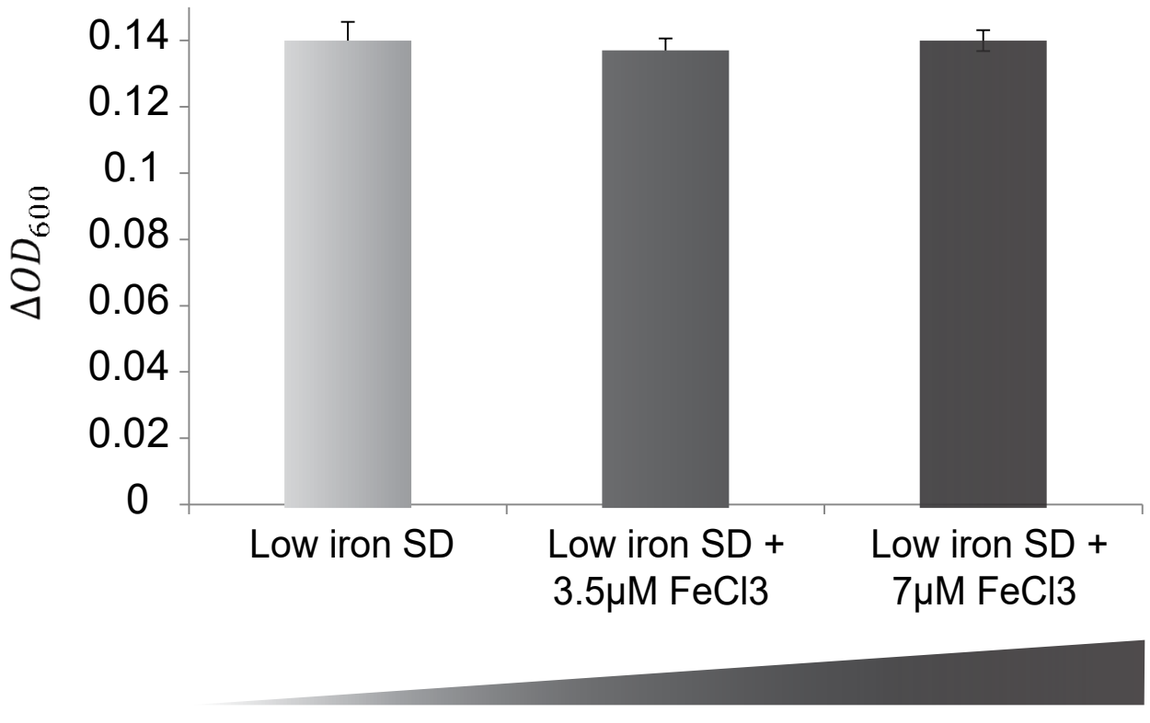

B

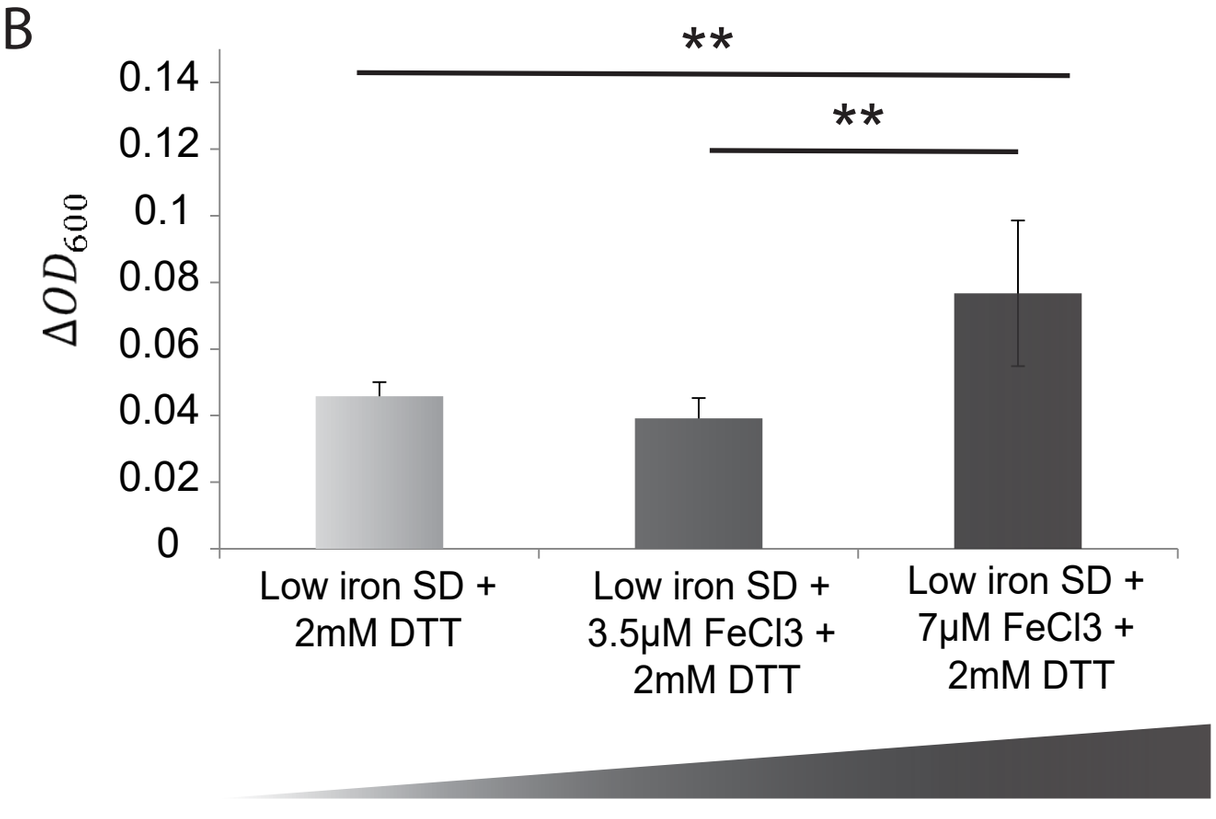

C

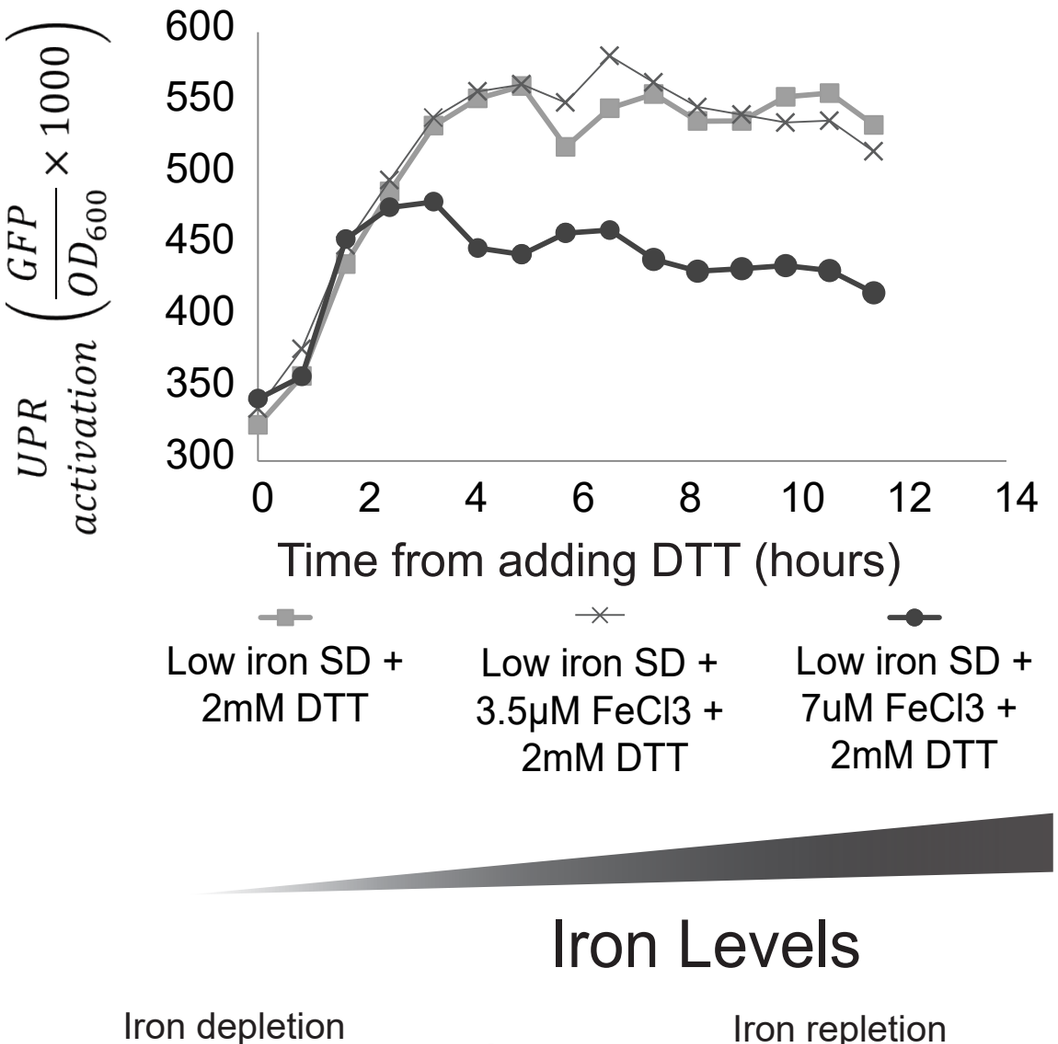

D

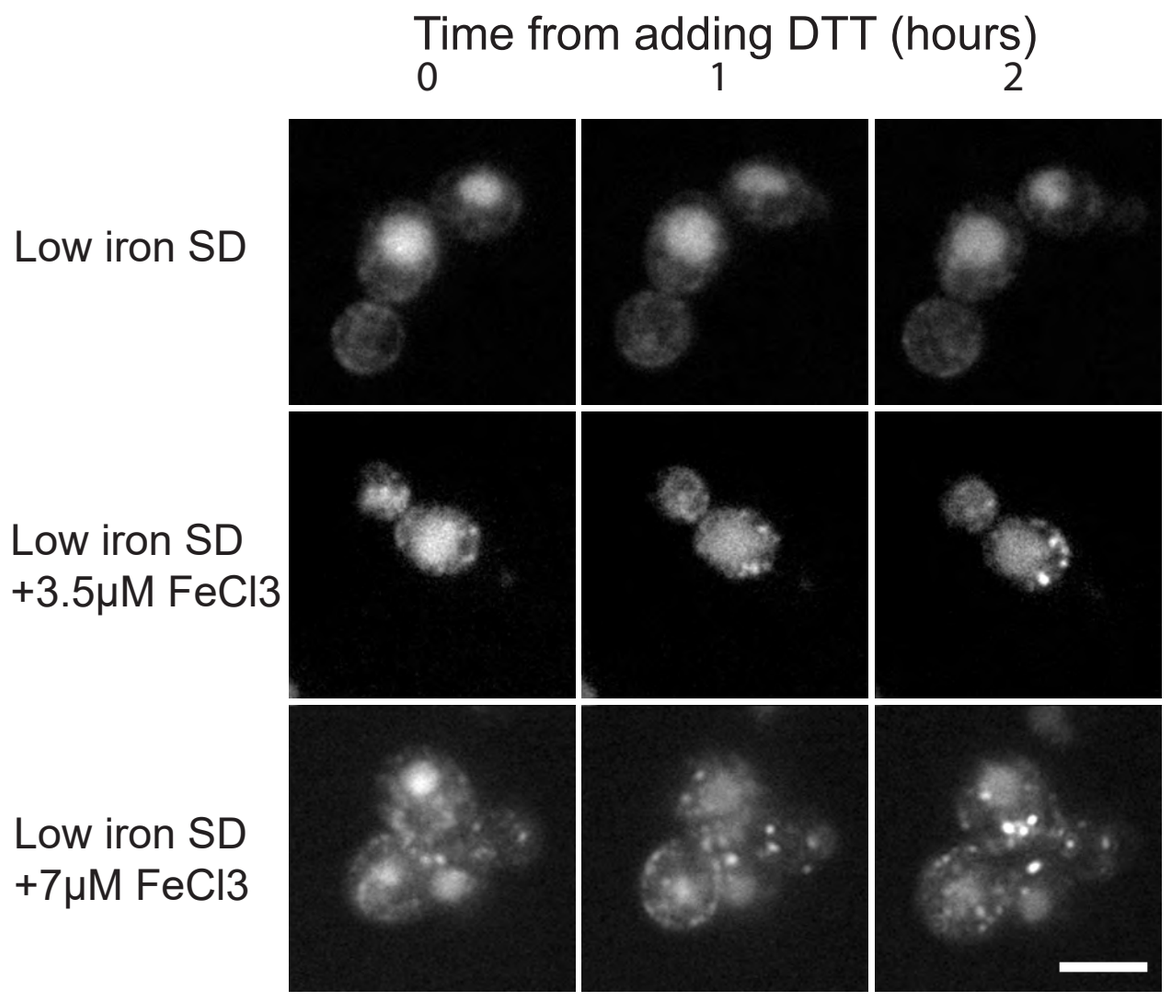

E

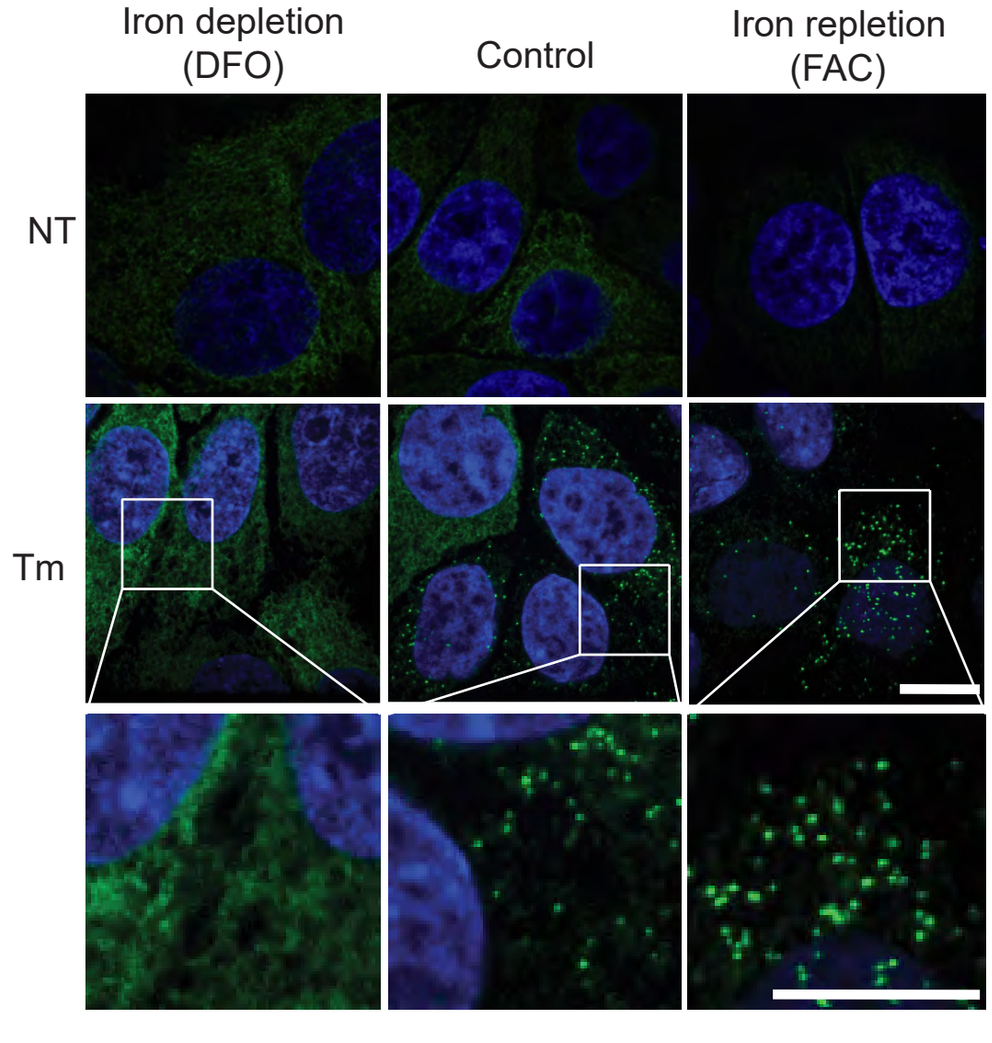

F

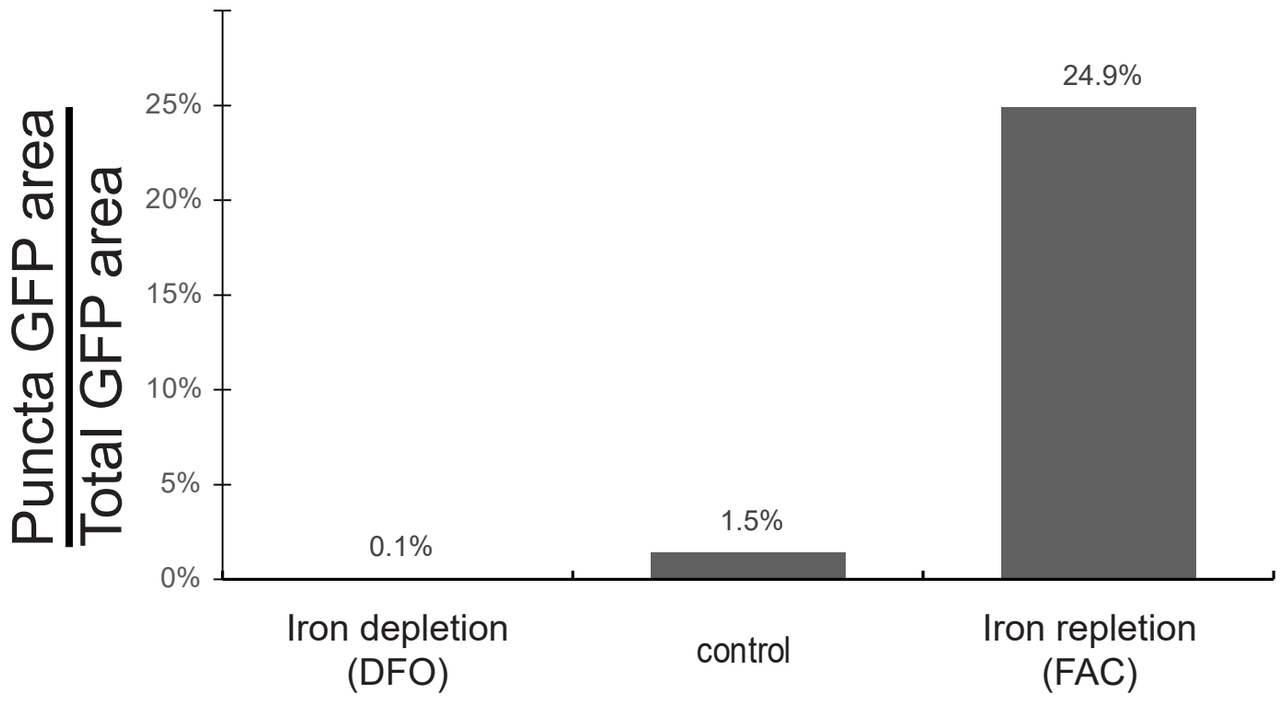

A

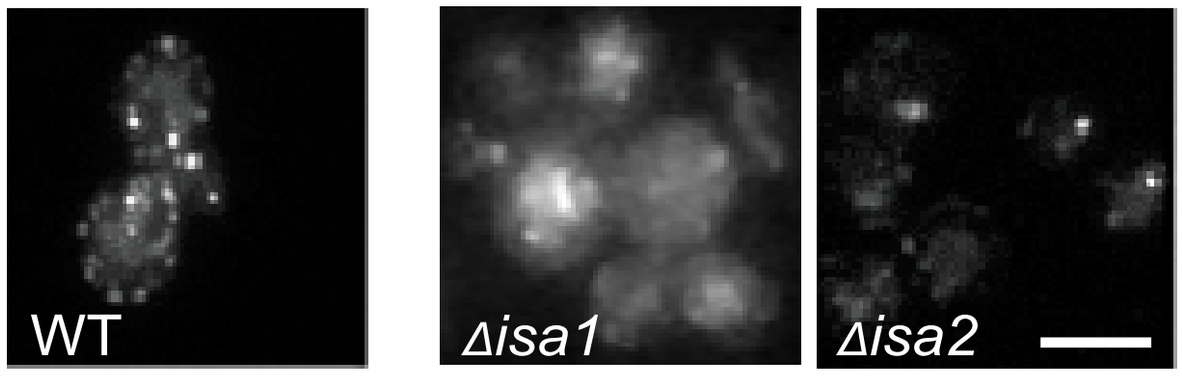

Iron sulfur cluster formation

B

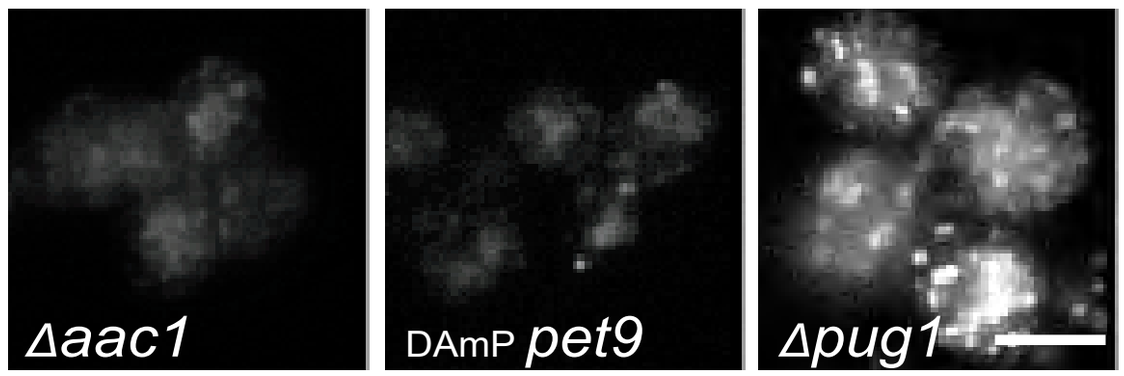

Afflux *Efflux*

Heme transporters

C

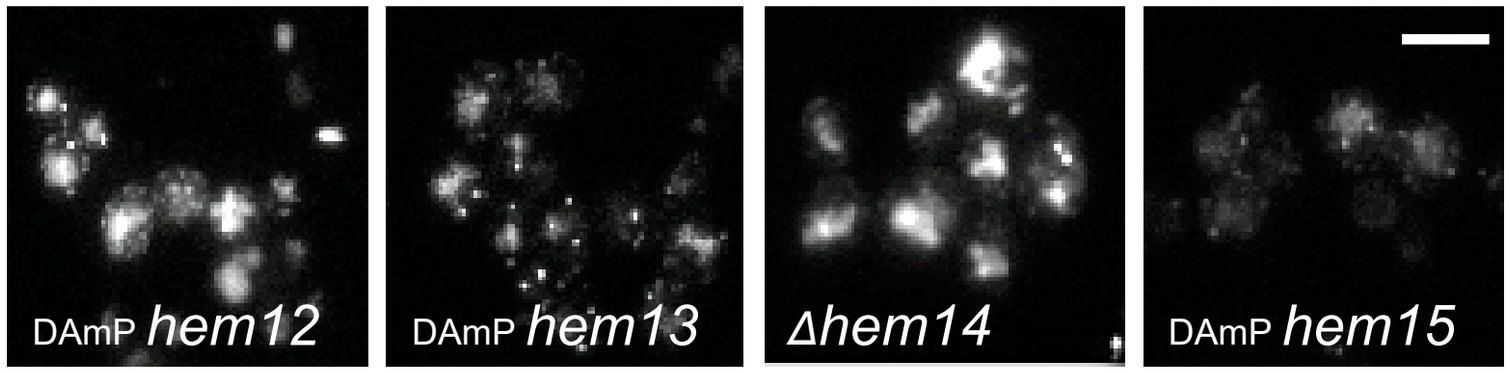

Heme biosynthesis

D

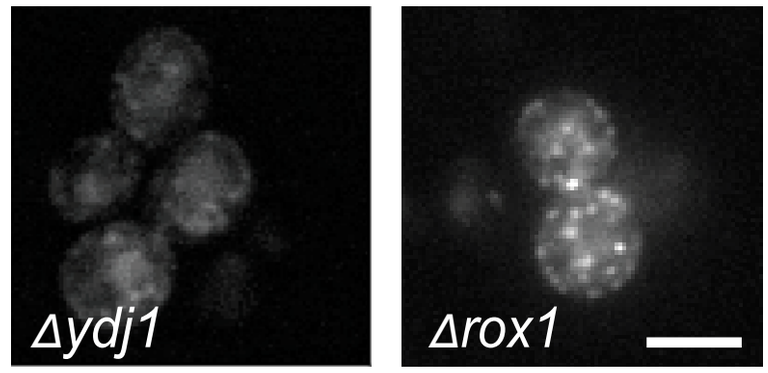

Heme regulators

E

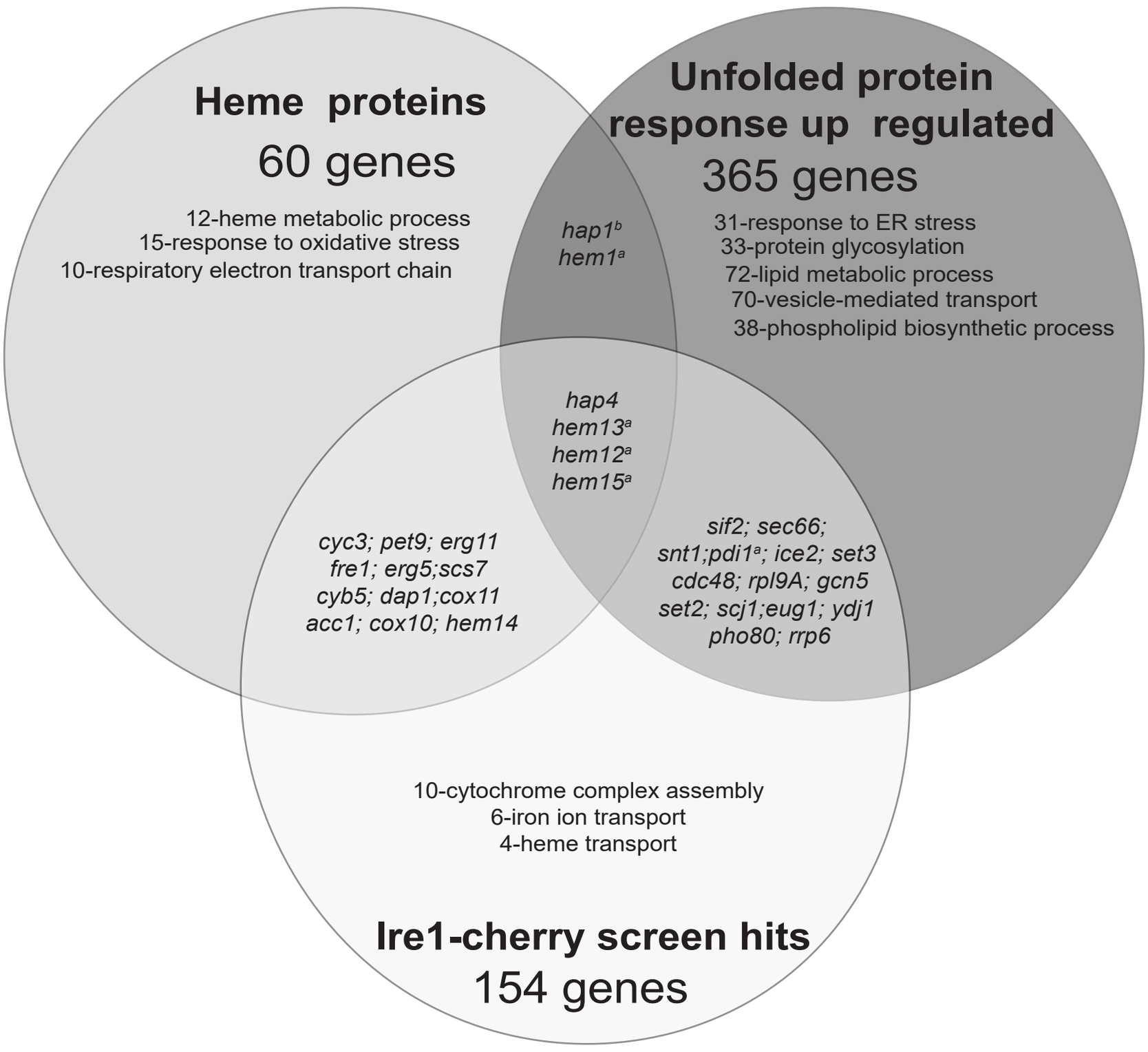

Cohen *et al*, Figure 5

A

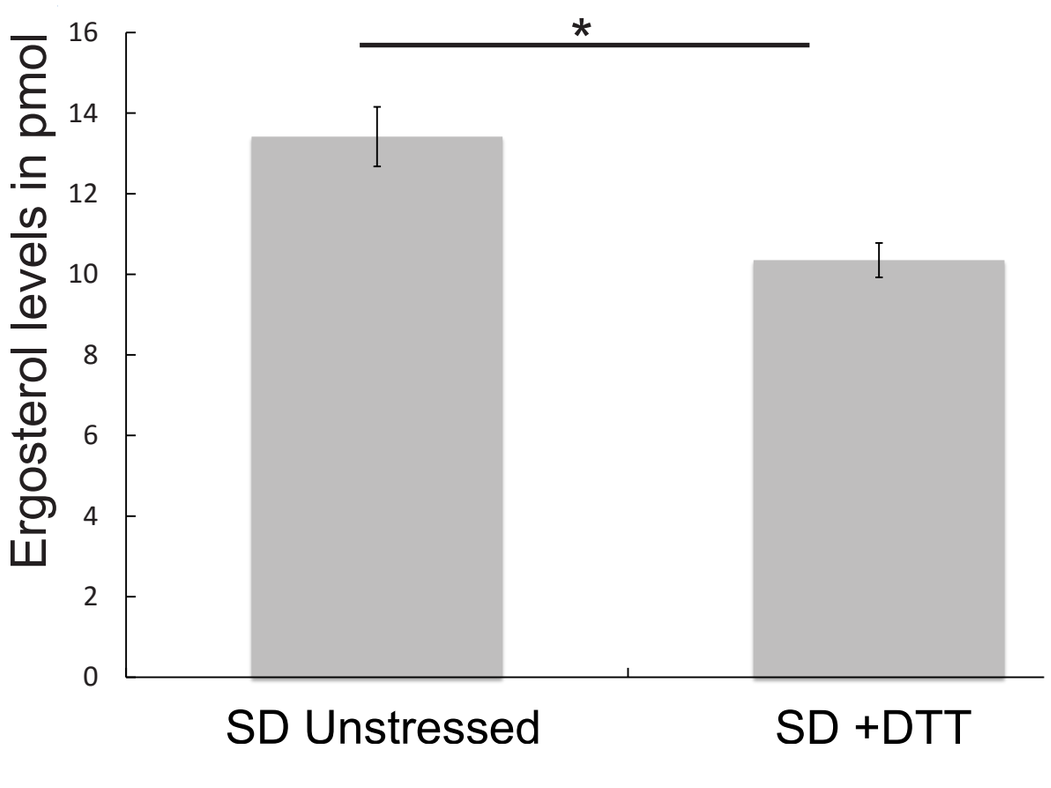

B

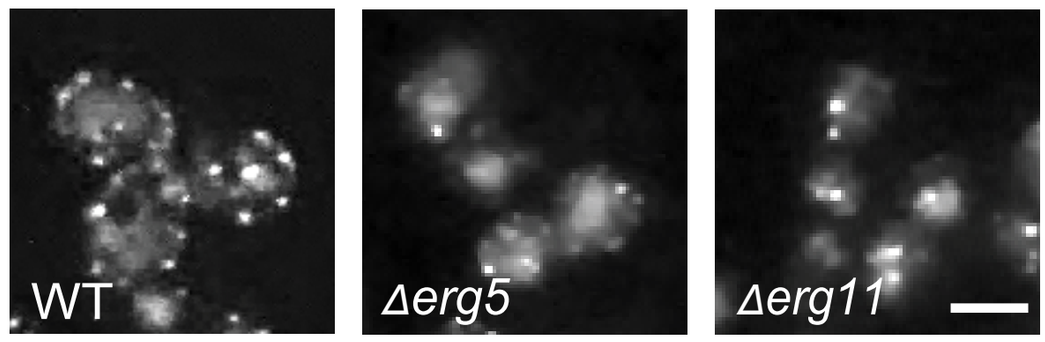

C

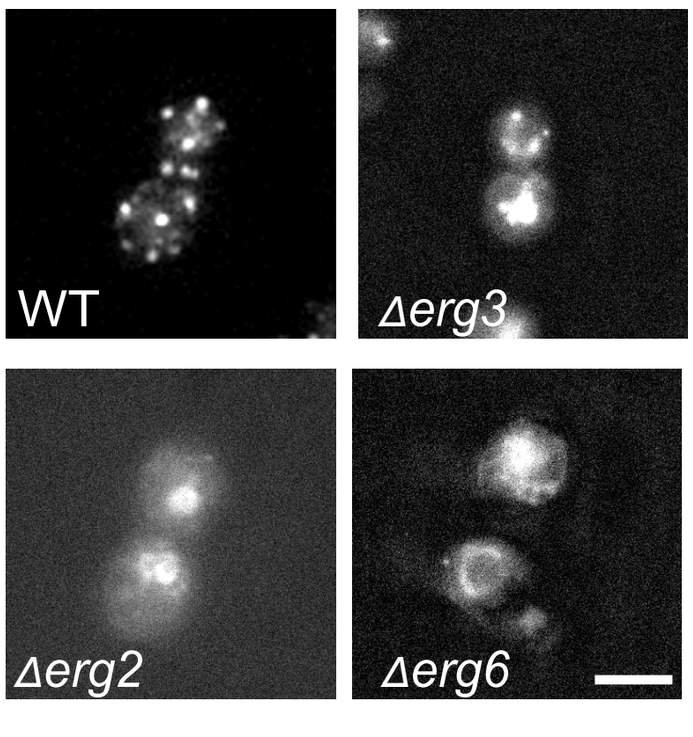

D

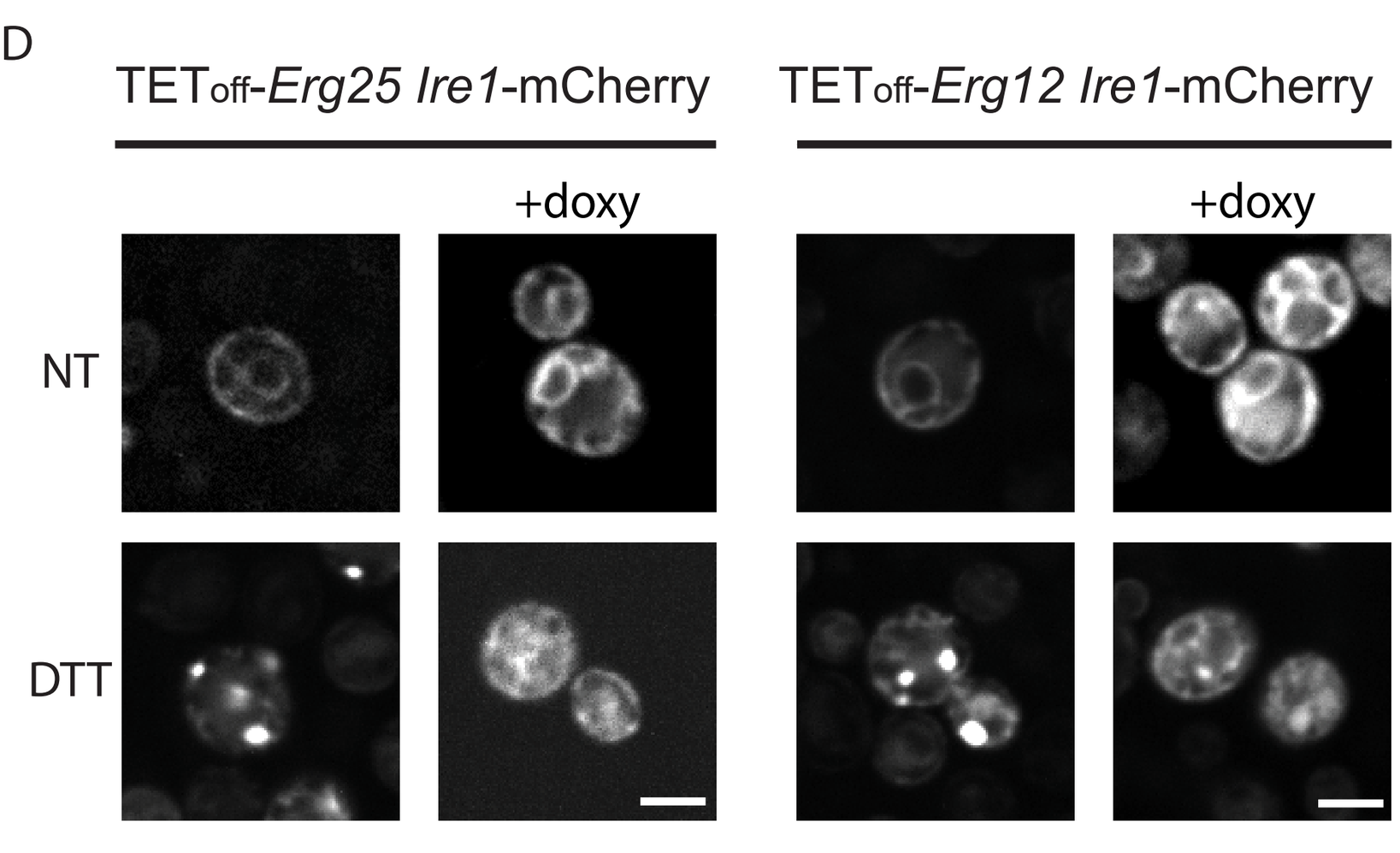

E

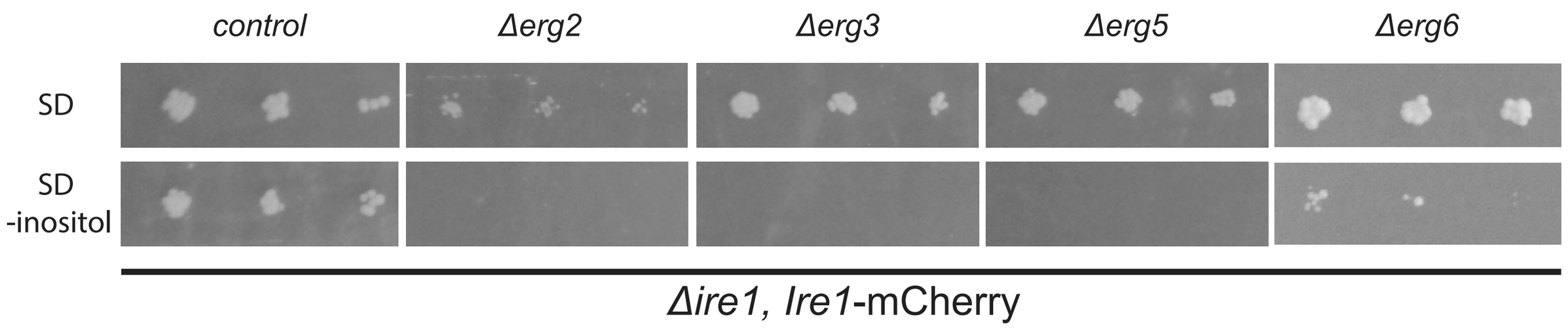

F

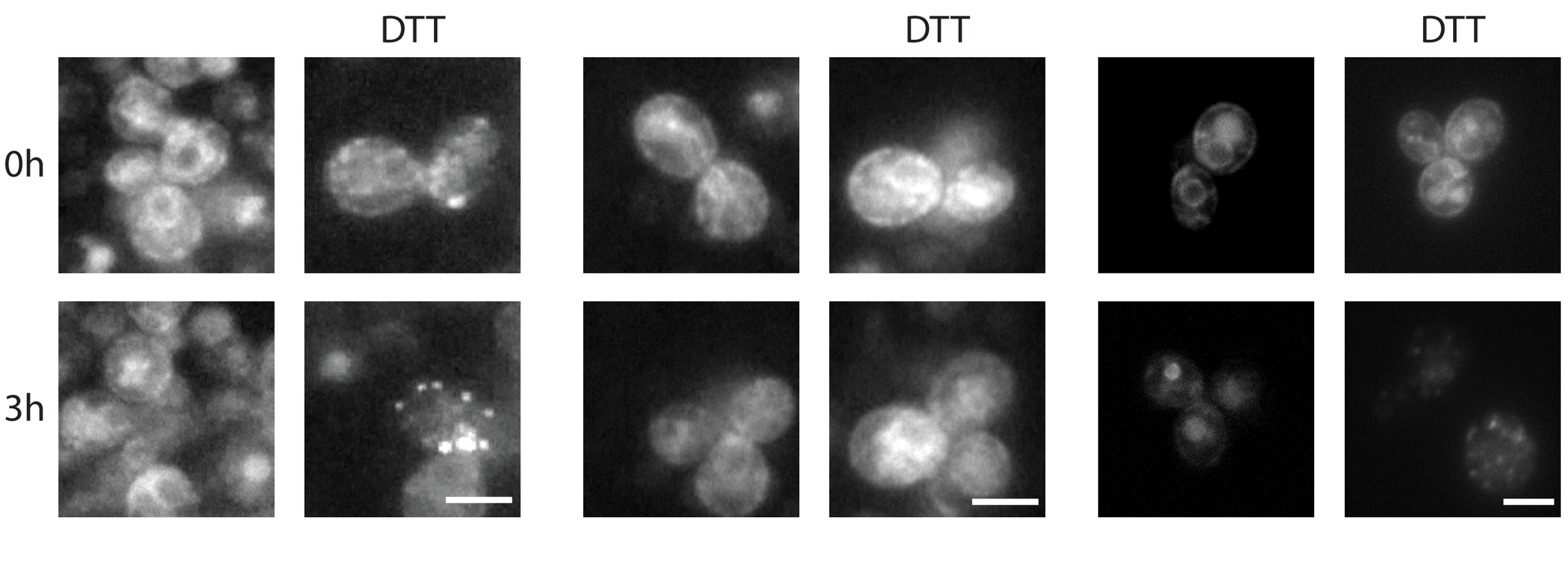

Cohen *et al*, Figure 6

A

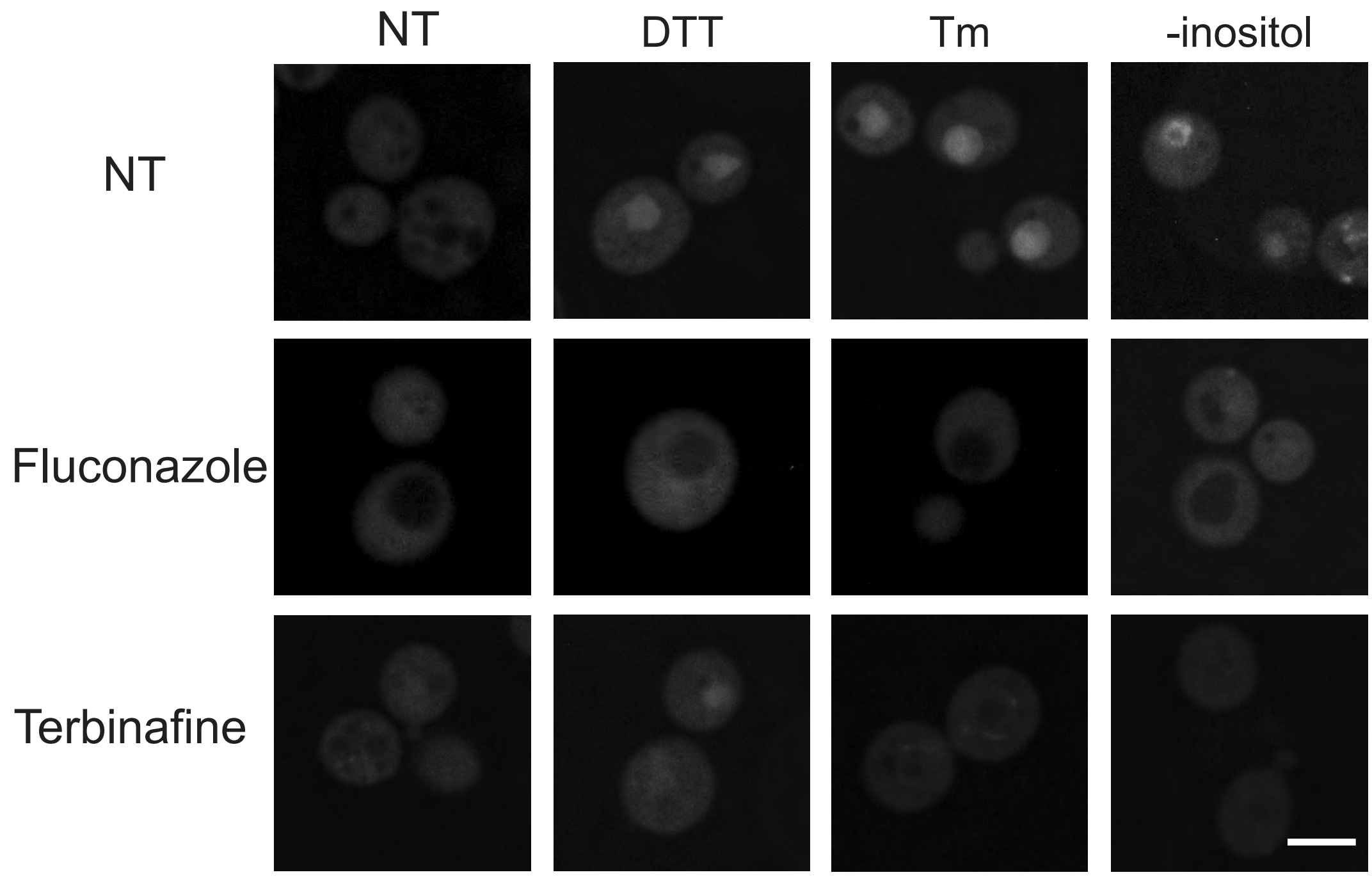

B

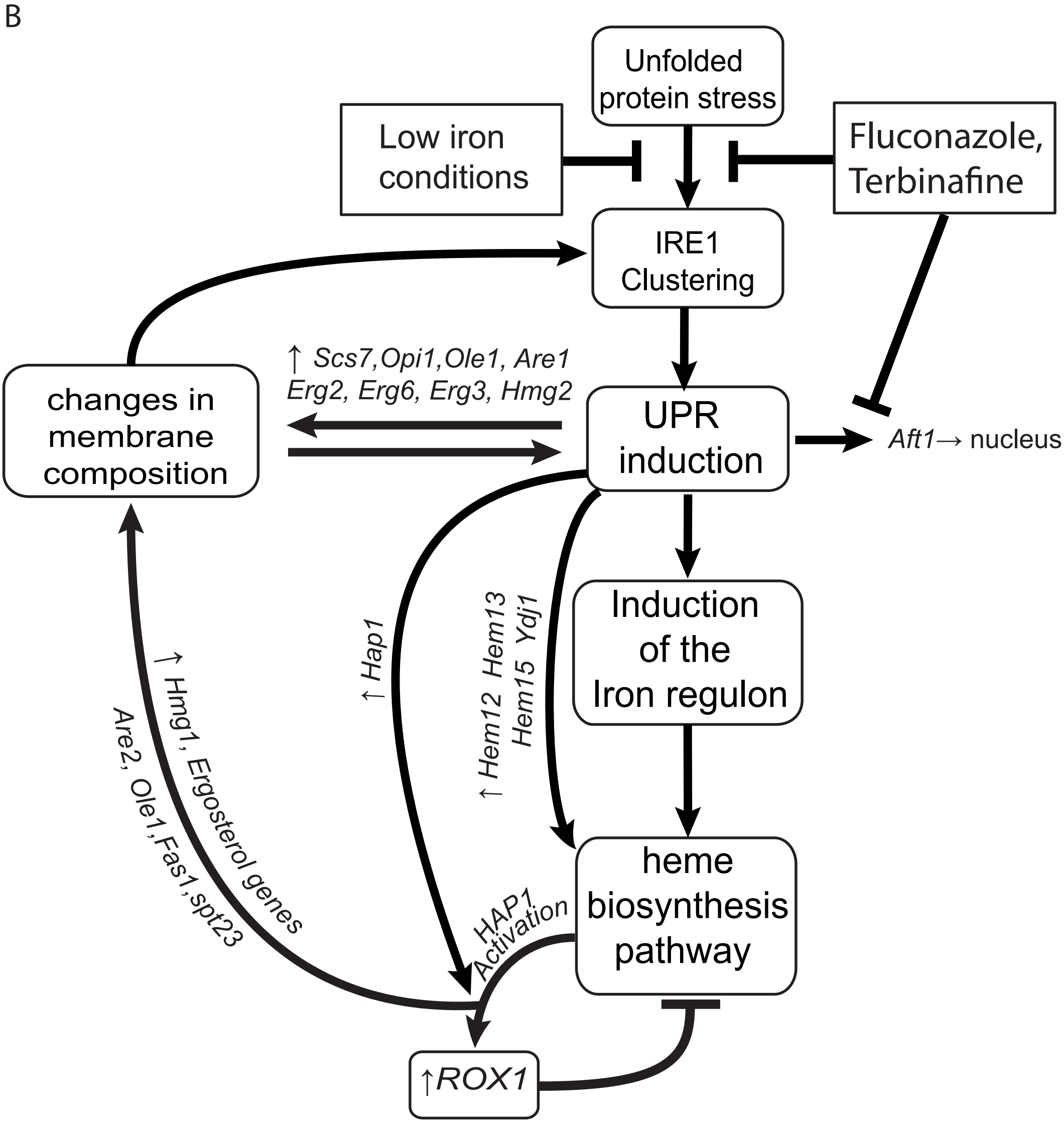

Cohen *et al*, Figure 1

A

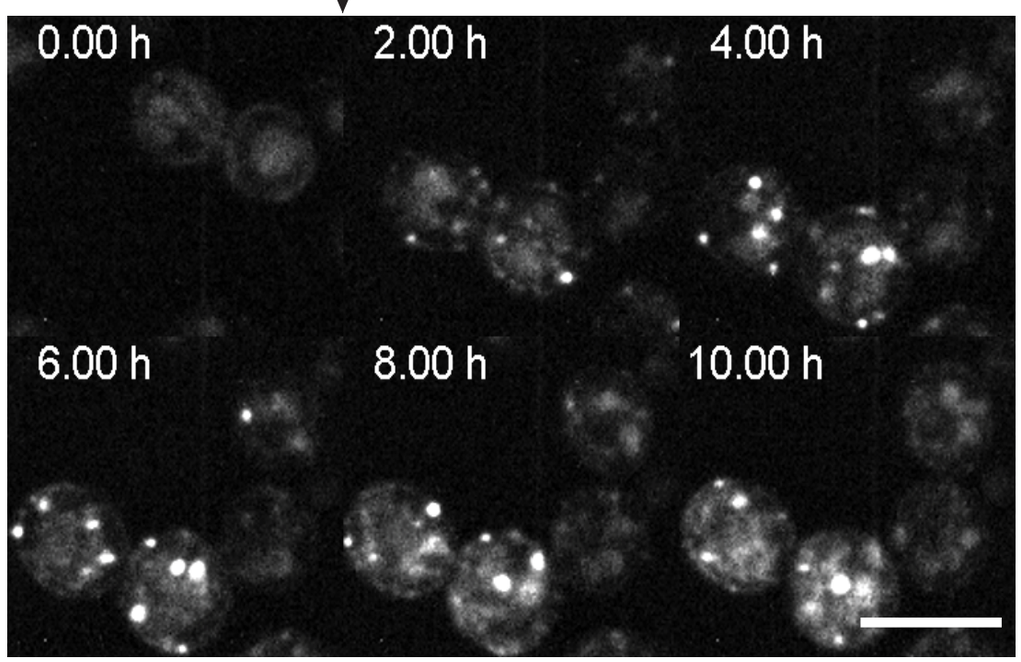

B

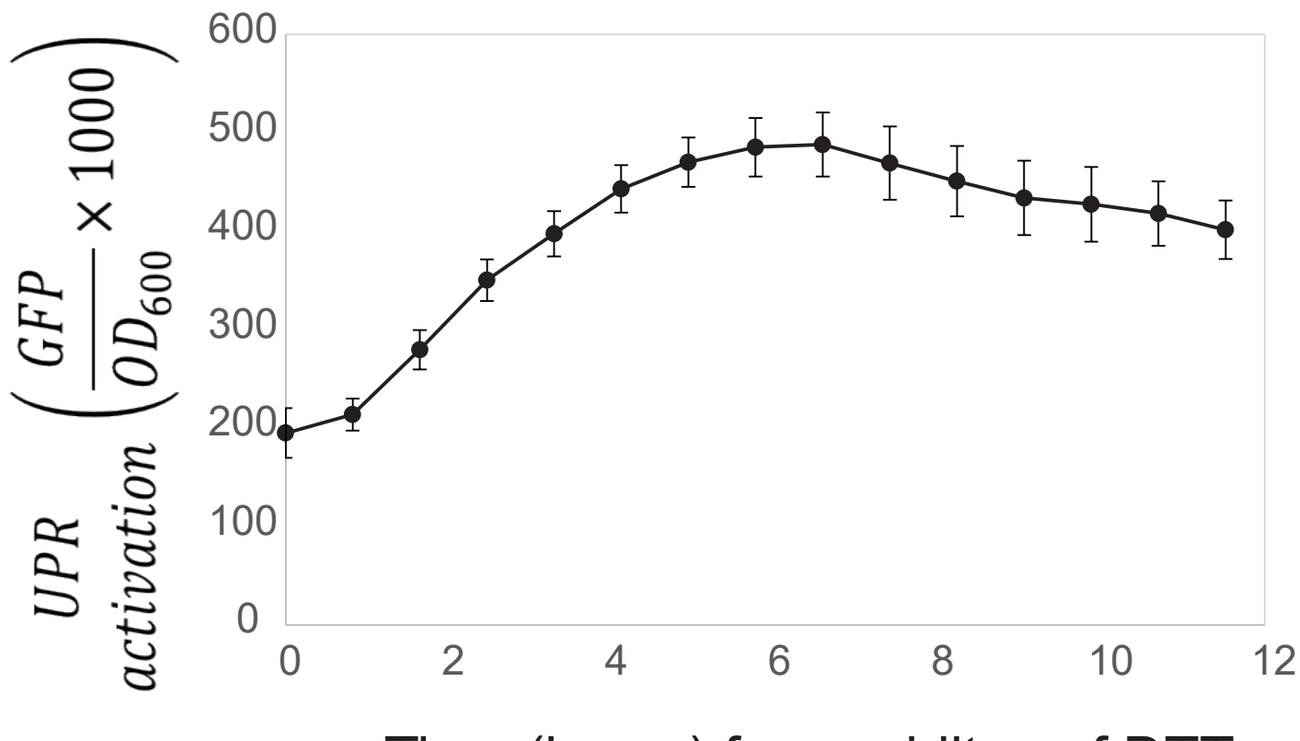

C

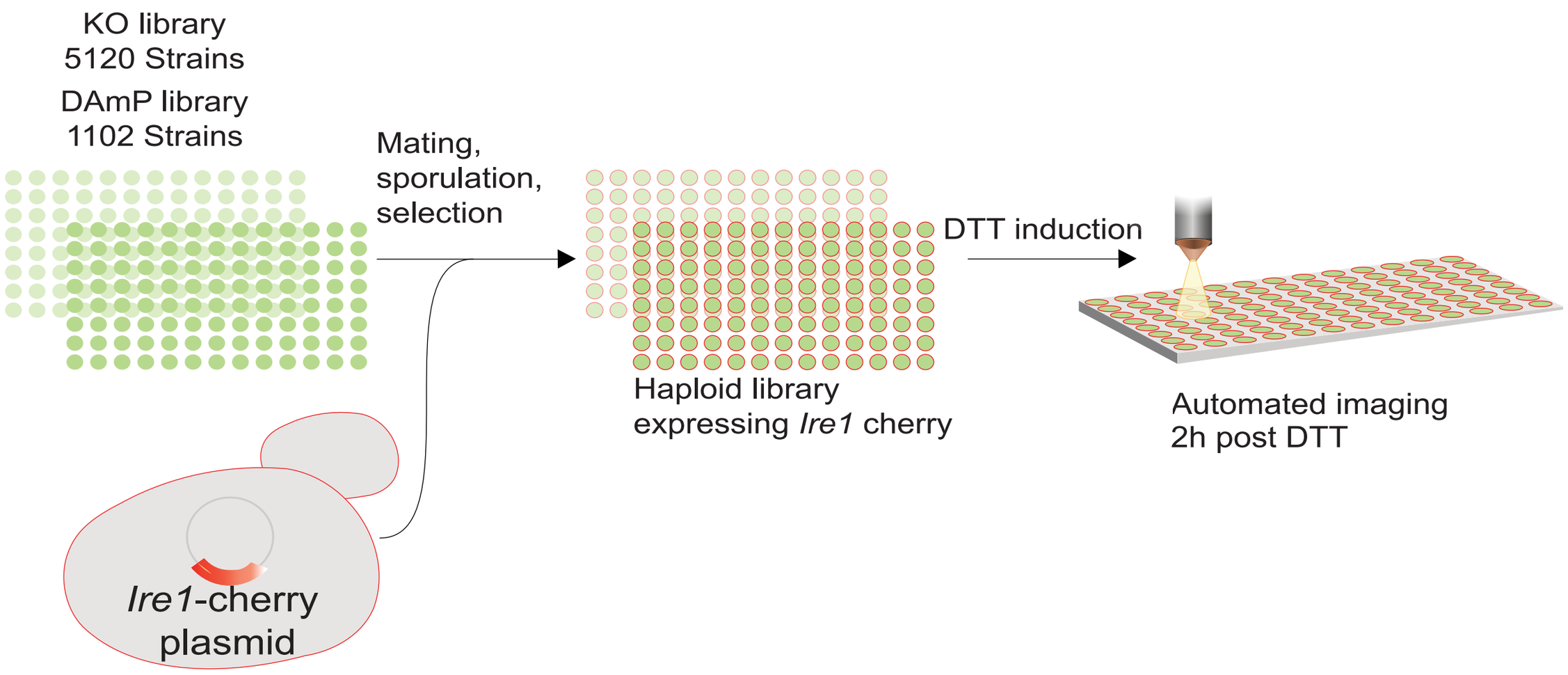

D